

**THE UNIVERSITY OF WESTERN ONTARIO  
DEPARTMENT OF CIVIL AND  
ENVIRONMENTAL ENGINEERING**

**Water Resources Research Report**

**Role of Remote Sensing in  
Disaster Management**

**By:  
Nirupama  
and  
Slobodan P. Simonovic**

**Report No. 040  
Date: July, 2002**

**ISSN: (print) 1913-3200; (online) 1913-3219;  
ISBN: (print) 978-0-7714-2610-0; (online) 978-0-7714-2611-7;**



# **ROLE OF REMOTE SENSING IN DISASTER MANAGEMENT**

By

Nirupama, Postdoctoral Fellow  
Department of Civil and Environmental Engineering  
University of Western Ontario, London, Ontario

And

Slobodan S. Simonovic, Professor and Research Chair  
Department of Civil and Environmental Engineering  
Institute for Catastrophic Loss Reduction  
University of Western Ontario, London, Ontario

Prepared for: Institute of Catastrophic Loss Reduction, London, Ontario

Date: July 2002

## TABLE OF CONTENTS

|       |  |    |
|-------|--|----|
| 1.    | INTRODUCTION .....   | 8  |
| 2.    | REMOTE SENSING TECHNOLOGY .....  | 12 |
| 2.1   | Satellites in Space .....  | 15 |
| 2.2   | Various Sensors and Their Applications .....                           | 27 |
| 3.    | DISASTER MANAGEMENT AND REMOTE SENSING.....                            | 32 |
| 3.1   | Earthquakes .....  | 34 |
| 3.2   | Volcanic Eruptions .....   | 35 |
| 3.3   | Tsunamis .....   | 40 |
| 3.4   | Hurricanes .....   | 41 |
| 3.5   | Landslides .....   | 44 |
| 3.6   | Floods.....  | 49 |
| 3.6.1 | Flood Mapping.....   | 53 |
| 3.6.2 | Flood Prediction Through Observation of Clouds .....                   | 59 |
| 3.6.3 | The Snow Factor .....  | 62 |
| 4.    | GEOGRAPHIC INFORMATION SYSTEM .....                                    | 67 |
| 5.    | WEB TECHNOLOGY .....   | 72 |
| 6.    | CASE STUDY .....   | 74 |
| 6.1   | Methodology .....  | 77 |
| 6.1.1 | Land use Classification of Satellite Imagery .....                     | 77 |
| 6.1.2 | Hydrologic data analysis .....   | 81 |
| 6.1.3 | Description of study area .....  | 82 |
| 6.2   | Data Analysis and Results .....  | 83 |
| 6.2.1 | Remote Sensing Data Analysis .....                                     | 83 |
| 6.2.2 | Hydrologic Data Analysis .....   | 85 |
| 6.2.3 | Integration of remote sensing images and hydrologic data analysis..... | 94 |
| 6.2.4 | Discussion of Results .....  | 95 |
| 7.    | CONCLUDING REMARKS.....  | 96 |

## LIST OF FIGURES

|   |    |
|---|----|
| Figure 1: Concept of a satellite sensing the globe through its on-board sensors .....                           | 14 |
| Figure 2: Electromagnetic Spectrum.....   | 14 |
| Figure 3: Lago Grande, Brazil, showing flood delineation.....   | 17 |
| Figure 4: LANDSAT image of outer banks of North Carolina, USA, showing after-effects of Hurricane Floyd .....   | 19 |
| Figure 5: A NOAA-AVHRR image showing a fire (red) visible in Pike National Forest, Colorado, USA .....          | 20 |
| Figure 6: SPOT image showing oil outflow area of Tokyo Bay taken on July 3, 1997 ..                             | 21 |
| Figure 7 ERS SAR images of 1996 volcanic eruption on the Vatnajökul glacier .....                               | 23 |
| Figure 8: MOS-1 image of sea of Japan taken on May 15-27, 1993, showing sea surface temperature .....           | 24 |
| Figure 9: IRS-1D image showing a panchromatic satellite scene covering Sarajevo airport .....                   | 25 |
| Figure 10: IKONOS four-meter resolution image of Cairo, Egypt .....   | 26 |
| Figure 11: QuackBird image of Tarpani, Sicily captured on February 4, 2002 .....                                | 28 |
| Figure 12: MOS – MESSR image of ash cloud on October 18, 1989 .....   | 31 |
| Figure 13: IRS-1C LISS image of Sarajevo airport captured on August, 24, 1998 .....                             | 32 |
| Figure 14: Earthquake in Bhuj, India captured by IKONOS on February 2, 2001 .....                               | 36 |
| Figure 15: Volcanic eruption.....   | 39 |
| Figure 16: Aerial photo of before and after tsunami hit an area .....   | 42 |
| Figure 17: Hurricane Bret that hit Texas on August 22, 1999 .....   | 43 |
| Figure 18: Development of a cyclone in the Indian Ocean captured by METEOSAT-5 between 5 and 9 June 1998 .....  | 44 |
| Figure 19: SPOT multispectral image acquired after a landslide on 29 November 2000.                             | 48 |
| Figure 20: Combination of ERS-1 (June 1998) and ERS-2 (August 1998) SAR imagery of Yangtse River in China ..... | 52 |
| Figure 21: LANDSAT-1 image of March 1973 Mississippi River flood .....  | 54 |
| Figure 22: SPOT PAN image acquired on July 18, 1993 – 10 meter resolution.....                                  | 55 |
| Figure 23: SPOT PAN image focused on West Alton at 10 meter resolution .....                                    | 56 |
| Figure 24: SPOT image of 1990 flood of Red River .....  | 58 |
| Figure 25: Red River flood in Manitoba captured on May 11, 1990 by Landsat .....                                | 59 |
| Figure 26: METEOSAT image in visible, infrared and water vapor bands .....                                      | 60 |
| Figure 27: Cloud classification by a neural network. ....   | 63 |
| Figure 28: The GOES-8 images of the northeastern U.S. on January 7, 1996 .....                                  | 64 |
| Figure 29: NOAA-12 AVHRR image captured in 1995 showing snow in red .....                                       | 67 |
| Figure 30: C factor map obtained for Swan Creek, Ohio, USA .....  | 69 |
| Figure 31: Aerial photos of two different years to assess the urbanization in the catchment .....               | 70 |
| Figure 32: Land use thematic layer .....  | 70 |
| Figure 33: Flood extent and depth .....   | 71 |
| Figure 34: Overlay of flooding scenario on remotely sensed scene of the area .....                              | 71 |
| Figure 35: Snow water equivalent image .....  | 74 |

|   |    |
|---|----|
| Figure 36: Upper Thames River Watershed in southern Ontario, Canada.....  | 76 |
| Figure 37: Maximum Likelihood procedure .....   | 79 |
| Figure 38: LANDSAT 1 Image classified for land use.....   | 86 |
| Figure 39: LANDSAT 5 Image classified for land use.....   | 88 |
| Figure 40: LANDSAT 7 Image classified for land use.....   | 88 |
| Figure 41: Plot of differences in observed peak flows at Thorndale and Byron.....                               | 89 |
| Figure 42: 1970 observed hydrographs at Byron and Thorndale and total precipitation at<br>London, Ontario.....  | 90 |
| Figure 43: 1976 observed hydrographs at Byron and Thorndale and total precipitation at<br>London, Ontario.....  | 90 |
| Figure 44: 1983 observed hydrographs at Byron and Thorndale and total precipitation at<br>London, Ontario ..... | 91 |
| Figure 45: 1984 observed hydrographs at Byron and Thorndale and total precipitation at<br>London, Ontario ..... | 91 |
| Figure 46: 1985 observed hydrographs at Byron and Thorndale and total precipitation at<br>London, Ontario ..... | 92 |
| Figure 47: 1988 observed hydrographs at Byron and Thorndale and total precipitation at<br>London, Ontario ..... | 92 |
| Figure 48: 1993 observed hydrographs at Byron and Thorndale and total precipitation at<br>London, Ontario ..... | 93 |
| Figure 49: 1995 observed hydrographs at Byron and Thorndale and total precipitation at<br>London, Ontario.....  | 93 |
| Figure 50: 1997 observed hydrographs at Byron and Thorndale and total precipitation at<br>London, Ontario ..... | 94 |

LIST OF TABLES

|  |    |
|--|----|
| Table 1 Detailed Description of Satellites and Sensors .....                 | 13 |
| Table 2: Land Use Classification Results for LANDSAT-1, 5 and 7 Images ..... | 84 |

## **EXECUTIVE SUMMARY**

The objective of this report is to review the existing satellites monitoring Earth's resources and natural disasters. Each satellite has different repeat pass frequency and spatial resolution (unless it belongs to the same series of satellites for the purpose of continuation of data flow with same specifications). Similarly, different satellites have different types of sensors on-board, such as, panchromatic, multispectral, infrared and thermal. All these sensors have applications in disaster mitigation, though depending on the electromagnetic characteristics of the objects on Earth and the nature of disaster itself. With a review of the satellites in orbit and their sensors the present work provides an insight to suitability of satellites and sensors to different natural disasters. For example, thermal sensors capture fire hazards, infrared sensors are more suitable for floods and microwave sensors can record soil moisture. Several kinds of disasters, such as, earthquake, volcano, tsunami, forest fire, hurricane and floods are considered for the purpose of disaster mitigation studies in this report. However, flood phenomenon has been emphasized upon in this study with more detailed account of remote sensing and GIS (Geographic Information Systems) applicability. Examples of flood forecasting and flood mapping presented in this report illustrate the capability of remote sensing and GIS technology in delineating flood risk areas and assessing the damages after the flood recedes. With the help of a case study of the Upper Thames River watershed the use of remote sensing and GIS has been illustrated for better understanding. The case study enables the professionals and planning authorities to realize the impact of urbanization on

river flows. As the urban sprawl increases with the increase of population, the rainfall and snow melt reaches the river channels at a faster rate with higher intensity. In other words it can be inferred that through careful land use planning flood disasters can be mitigated.

Keywords: Remote sensing, GIS, land use change, Thames River Basin, flood disaster, satellite data.



## **ACKNOWLEDGEMENTS**

Funding from the Institute for Catastrophic Loss Reduction (ICLR) to carry out this work is gratefully acknowledged. Upper Thames River Conservation Authority (UTRCA) helped greatly in providing the necessary hydraulic GIS data for the case study.

## **1. INTRODUCTION**

The space technology and disaster mitigation communities work together in developing effective and accurate methods for prevention, preparedness and relief measures. Disaster prevention is a long-term phenomenon, which can best be studied with the help of satellite monitoring of various relevant factors, such as, changing land use. Disaster preparedness focuses on warnings and forecasts of impending disasters and often entails processes, which are quite dynamic and result in "rapid onset" disasters. Most disasters are of this type although some, such as drought and famine are slow to develop. The obvious difference between warnings and forecasts is that the latter is less specific in time and space. Disaster relief occurs after (and sometimes during) the emergency. An important aspect in terms of satellite monitoring involves assessment of the damage incurred during the disaster. Satellite technology can also help in identifying escape routes and locations for storage of temporary housing. The pressure on the earth's resources caused by increased population has resulted in increased vulnerability of human and their infrastructure to the natural hazards. The result is a dynamic equilibrium between these forces in which scientific and technological development plays a major role. Societal factors, such as, economics, politics, communication and education are vital in order to implement the technological advances.

Remote sensing or Earth Observation System (EOS) and GIS are among many tools available to disaster management professionals today making the effective project planning very much possible and more accurate now than ever before. Although none of

the existing satellites and their sensors has been designed solely for the purpose of observing natural hazards, the variety of spectral bands in VIS (visible), NIR (near infrared), IR (infrared), SWIR (short wave infrared), TIR (thermal infrared) and SAR (Synthetic Aperture Radar) provide adequate spectral coverage and allow computer enhancement of the data for this purpose. Repetitive or multi-temporal coverage is justified on the basis of the need to study various dynamic phenomena whose changes can be identified over time. These include natural hazard events, changing land use-patterns, and hydrologic and geologic characteristics of the region.

In disaster management, the aim of the experts (Kundzewicz et al, 1993; Lanza and Conti, 1994; Sabins, 1986) has been to monitor the situation, simulate the complicated natural phenomenon as accurately as possible so as to come up with better prediction models, suggest appropriate contingency plans and prepare spatial databases.

From the inherent characteristics, namely, spatial continuity, uniform accuracy and precision, multi-temporal coverage and complete coverage regardless of site location, the remotely sensed data can be used very effectively, for:

- Quickly assessing severity and impact of damage due to flooding, earthquakes, oil spills and other disasters;
- Planning efficient escape routes from coastal areas during hurricane season;
- Charting quickest routes for ambulances to reach victims;
- Locating places for shelter for victims or refugees;

- Calculating population density in disaster-prone areas;
- Rapidly identifying hardest-hit disaster areas in order to provide early warning of potential disasters;
- Pre-disaster assessments to facilitate planning for timely evacuation and recovery operations during a crisis;
- Monitoring reconstruction or rehabilitation after a major disaster; and
- Developing, maintaining or updating accurate base maps.

Different sensors can provide unique information about properties of the surface or shallow layers of the Earth. For example, measurements of the reflected solar radiation give information on albedo (fraction of light that is reflected by a body or surface), thermal sensors measure surface temperature, and microwave sensors measure the dielectric properties and hence, the moisture content, of surface soil or of snow. Remote sensing and its continued development have added new techniques that disaster management experts can use in a large number of applications.

This work includes a review of the existing Earth resource satellites in orbit, which are of great help for disaster mitigation studies. Sensors and their capabilities with reference to disaster mitigation are discussed in separate sections. A case study, conducted on the Upper Thames River watershed (mainly monitoring the extent of major urban development around the city of London) illustrates the use of satellite data to monitor changing land use and its impact on river channel flows over the last three decades.

## **2. REMOTE SENSING TECHNOLOGY**

The Earth observation using satellite remote sensing technique has made it possible to obtain uniform data covering the whole globe in a relatively short time, and has also made it possible for these observations to be continued for a long time in the future (Figure 1). The two main components of the space-based sub-system of the EOS, Polar-Orbiting and Geostationary, continue to improve with every new launch. Geostationary satellites orbit the earth with the earth's rotation so that they observe the same point on the Earth continuously, but from a much higher altitude approaching 36,000 km. Geostationary satellites are the primary meteorological observation platforms and provide continuous but somewhat coarser spatial data. Polar orbiting satellites generally fly in a low Earth orbit (hundreds of km) and provide relatively high resolution measurements with repeat times of days to tens of days. Typical polar orbiting satellites (Table 1) are the NOAA-AVHRR, the French SPOT and the US LANDSAT and TM series. The data received from polar-orbiting satellites is very useful in understanding and monitoring the natural hazards. Also, the effect of the space and time distribution of water accompanied by phase changes on the water and energy budget at the earth surface from the point of view of understanding and control of the mechanism of environmental changes can be better evaluated with satellite data.

Remote sensing data are acquired in predetermined spectral bands (wave lengths). Visible

Table 1 Detailed Description of Satellites and Sensors

| Satellite | Country | Repeat cycle                                 | Sensor  | Frequency/Band (microns)  | Resolution                             | Swath (km)            |           |  |
|-----------|---------|--|---|---|--|-----------------------|-----------|--|
| RADARSAT  | Canada  | 24 days                                      | SAR   | 5.3 GHz (C-Band)  | Standard resolution<br>Fine resolution | 28 x 25 m<br>10 x 9 m | 100<br>45 |  |
| LANDSAT   | USA     | 16 days                                      | TM/ETM  | 0.45-0.52, 0.52-0.60, 0.63-0.69<br>0.76-0.90, 1.55-1.75, 2.08-2.35  | 30 m                                   | 185                   |           |  |
|           |         |  | MSS   | 0.5-0.6, 0.6-0.7, 0.7-0.8, 0.8-1.1, 10.4-12.6   | 79 m                                   | 185                   |           |  |
|           |         |  | MTB   | 10.4-12.5   | 60 m                                   |                       |           |  |
|           |         |  | PAN   | 0.5-0.9   | 15 m                                   |                       |           |  |
| SPOT      | France  | 26 days<br>(5 days with pointing capability) | HRVIR (1)   | 0.50-0.59, 0.61-0.68, 0.79-0.89, 1.58-1.75  | 20 m                                   | 60                    |           |  |
|           |         |  | HRVIR (2)   | 0.61-0.68   | 10 m                                   | 60                    |           |  |
|           |         |  | VMI   | 0.43-0.47, 0.50-0.59, 0.61-0.68, 0.79-0.89, 1.58-1.75   | 1 m                                    | 2000                  |           |  |
| ERS       | Europe  | 35 days                                      | AMI Active Microwave Instrumentation                              |   |  |                       |           |  |
|           |         |  | SAR Image   | 5.3 GHz (C-Band)  | <30 m                                  | 80-100                |           |  |
|           |         |  | SAR Wave  | 5.3 GHz (C-Band)  | <30 m                                  | 5                     |           |  |
|           |         |  | Scatterometer   | 5.3 GHz (C-Band)  | 50 km                                  | 500                   |           |  |
|           |         |  | Radar Altimeter   | 13.5 GHz (KU-Band)  | 10cm accuracy                          |                       |           |  |
|           |         |  | ATSR-M Along Track Scanning Radiometer with Microwave Sounder     |   |  |                       |           |  |
|           |         |  | Infrared Radiometer   | 1.6, 3.7, 11, 12  | 1 km x 1 km                            | 500                   |           |  |
|           |         |  | Microwave sounder   | 23.5 (GHz)  | 22 km                                  | 500                   |           |  |
| NOAA      | USA     | 12 hr  | AMSU-A  | 23.8 (GHz), 31.4, 50.3, 52.8, 53.33, 54.4, 54.94, 55.5, 57.29 (6 channels), 89.0  | 40 km                                  | 2240                  |           |  |
|           |         |  | AMSU-B  | 89.0, 166.0, 183.31 (3 channels)  | 15 km                                  | 2240                  |           |  |
|           |         |  | AVHRR/3   | 1) 0.58-0.68, 2) 0.72-1.00, 3A) 1.58-1.64 (day), 3B) 3.55-3.93 (night), 4) 10.3-11.3, 5) 11.5-12.5  | 0.5 km (VIS)<br>1.0 km (IR)            | 2940                  |           |  |
|           |         |  | HIRS-3<br>20 IR Bands<br>(Microns)<br>(Wavelength at band center) | (1) 14.95, (2) 14.71, (3) 14.49, 4) 14.22<br>(5) 13.97, (6) 13.64, (7) 13.35, 8) 11.11<br>(9) 9.71, (10) 12.47, (11) 7.33, 12) 6.52<br>(13) 4.57, (14) 4.52, (15) 4.47, 16) 4.45<br>(17) 4.13, (18) 4.00, (19) 3.76, 20) 0.69 | 17.4 km                                | 2240                  |           |  |
| MOS       | Japan   | 17   | MESSR   | 0.51-0.59, 0.61-0.69, 0.72-0.80, 0.80-1.1   | 50 m                                   | 100                   |           |  |
|           |         |  | VTIR (1)  | 0.5-0.7, 6.0-7.0  | 0.9 km                                 | 1500                  |           |  |
|           |         |  | VTIR (2)  | 10.5-11.5, 11.5-12.5  | 2.7 km                                 | 1500                  |           |  |
|           |         |  | MSR (1)   | 23.8GHz   | 32 km                                  | 317                   |           |  |
| JERS      | Japan   | 44   | SAR   | 1275 MHz (L-Band)   | 18 m x 18 m                            | 75                    |           |  |
|           |         |  | OPS<br>VNIR<br>SWIR   | (1) 0.52-0.60<br>(2) 0.63-0.69, (3) 0.76-0.86*, (4) 1.60-1.71** (5) 2.01-2.12<br>(6) 2.13-2.25, (7) 2.27-2.40   | 18 m x 24 m                            |                       |           |  |
| IRS       | India   | 24   | LISS-III<br>VNIR  | 0.52-0.59<br>0.62-0.68, 0.77-0.86   | 23m                                    | 142                   |           |  |
|           |         | 5  | SWIR  | 1.55-1.70   | 70.5                                   | 148                   |           |  |
|           |         | 5  | PAN<br>WiFS   | 0.50-0.75, 0.62-0.68<br>0.77-0.86   | 5.8m<br>188m                           | 70<br>774             |           |  |
| IKONOS    | USA     | 2.9  | PAN   | 0.45 - 0.90   | 1m                                     | 11km                  |           |  |
|           |         | 1.5  | VNIR  | 0.45 - 0.52, 0.52 - 0.60<br>0.63 - 0.69, 0.76 - 0.90  | 4m                                     |                       |           |  |
| QuickBird | USA     | 3.5  | PAN<br>MULTISPECTRAL  | 0.45 - 0.9<br>0.45 - 0.52, 0.52 - 0.6, 0.63 - 0.69, 0.76 - 0.9  | 61cm<br>2.44m                          | 16.5km                |           |  |

AATSR Advanced Along Track Scanning Radiometer  
AMSU-A Advanced Microwave Sounding Unit-A  
AMSU-B Advanced Microwave Sounding Unit-B  
AVHRR/3 Advanced Very High Resolution Radiometer  
ETM Enhanced thematic Mapper  
GOME Global Ozone Monitoring Experiment  
band 3 and 4 make stereo pair

HIRS-3 High Resolution Infrared Radiation Sounder  
HRVIR High Resolution Visible Infrared  
IR Infrared  
MESSR Multispectral Electronic Self -Scanning Radiometer  
MTB Multispectral Thermal Band  
MSR Microwave Scanning Radiometer  
band 4 is for forward viewing (15.33 degrees)

OPS Optical Sensors  
PAN PANchromatic  
SAR Synthetic Aperture Radar  
VIS Visible  
VMI Vegetation Monitoring Instrument  
VTIR Visible And Thermal-Infrared Radiometer

and near infrared spectral bands (which can be displayed as colors as shown in Figure 1) are chosen to amplify or separate specific earth features such as vegetation, rocks, urban area, snow and water. This way one can separate a chosen land feature from other land features by choice of the wavelength.

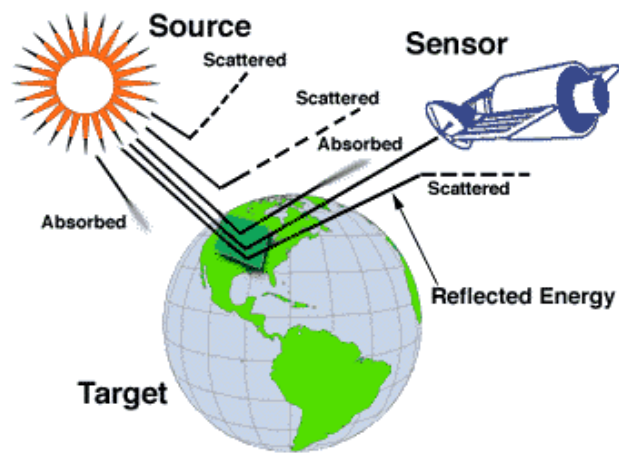


Figure 1: Concept of a satellite sensing the globe through its on-board sensors

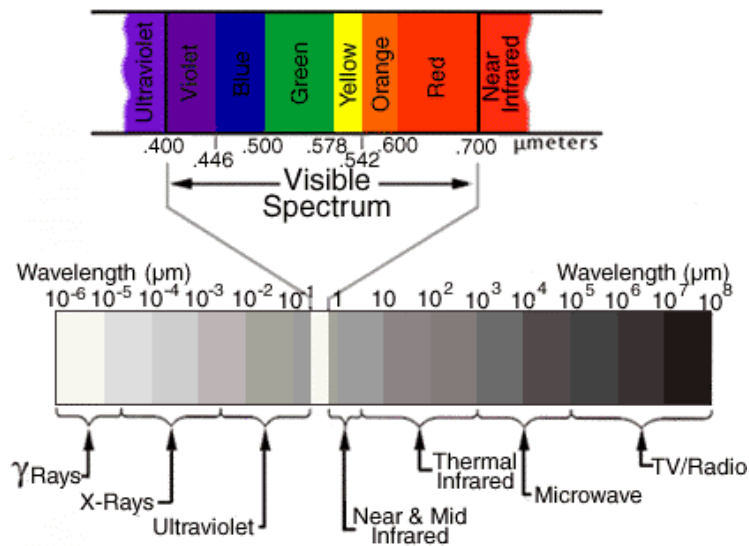


Figure 2: Electromagnetic Spectrum

In the following sections the focus will be on polar orbiting satellites, which are more relevant to natural hazards. Some of the prominent polar orbiting satellites are listed in Table 1. Few of the many agencies receiving/distributing the data from the above listed satellites are:

- i) RadarSat International (RSI), Canada;
- ii) Canada Center for Remote Sensing, Canada;
- iii) Center for Remote Imaging, Sensing and Processing (CRISP), Singapore;
- iv) EROS Data Center (EDC), USA;
- v) Space Imaging, USA;
- vi) SPOT Imaging, France; and
- vii) National Remote Sensing Agency (NRSA), India.

## **2.1 Satellites in Space**

RADARSAT, the Canadian satellite uses SAR, an active microwave sensor, allowing 24-hour data collection, independent of weather conditions and illumination. The SAR sensor has selective viewing angles that allow a wide range of terrain conditions, applications and ground coverage requirements to be accommodated. Imaging modes for RADARSAT (Table 1) include Fine, Standard, Wide, ScanSAR (narrow and wide), and Extended Beam (high and low incidence angles). RADARSAT has proven to be the most efficient and effective satellite sensor for detecting flood damages and oil seeps. It is estimated that over \$500 million in dry holes have been avoided because of RADARSAT



seep detection. In the following image shown in Figure 3 an excellent land/water delineation can be seen. The forest adjacent to Lago Grande, Brazil experience seasonal flooding, and the dark areas on this image represent the high water mark and flooded areas, while the forested areas are of a lighter tone.

The LANDSAT program is the longest running exercise in the collection of multispectral digital data of the Earth's surface from space. Since LANDSAT 1 (then Earth Resources Technology Satellite) was launched on July 23, 1972, data is being collected in a continuous stream, through one after another launch of LANDSAT (LANDSAT 7 is the latest in orbit), along a near vertical path as the satellite moves from north to south. LANDSAT path designations increase from east to west. The MSS (Multi Scanner System) sensor scans the Earth's surface from west to east as the satellite moves in its

descending (north-south) orbit over the sunlit side of the Earth. Six detectors for each spectral band provide six scan lines on each active scan. The combination of scanning geometry, satellite orbit, and Earth rotation produce the global coverage necessary for studying land surface change. There are ground stations to record LANDSAT data all over the world ([www.geoimage.com.au](http://www.geoimage.com.au), and [www.gsfc.nasa.gov](http://www.gsfc.nasa.gov)). Figure 4 is an example of LANDSAT 7 image acquired on September 23, 1999 showing the after-effects of hurricane Floyd.

NOAA (National Oceanic and Atmospheric Administration), in the United States of America, over past 25 years, have made important strides in understanding and predicting



Figure 3: Lago Grande, Brazil, showing flood delineation(source:<http://www.space.gc.ca>)

the behavior of natural systems, in managing resources more effectively, and in improving environmental quality. NOAA operates LANDSAT 7 with the National Aeronautics and Space Administration (NASA) and the U. S. Geological Survey (USGS). NOAA's Polar Orbiting Environmental Satellites (POES) are operating since 1978. The EROS Data Center (EDC) AVHRR (Advance Very High Resolution Radiometer) Data Acquisition and Processing System (ADAPS), which began operation in May 1987, receives approximately six daytime passes per day of HRPT (High Resolution Picture Transmission) data over the conterminous United States, while the night acquisitions are acquired upon request only ([edc.usgs.gov/glis/hyper/](http://edc.usgs.gov/glis/hyper/)). Detailed description of AVHRR sensor is given in the following sections and in Table 1. Figure 5 is an example of a

NOAA-AVHRR imagery taken on June 18, 2002 showing a large heat signatures (red) and smoke plume (light blue haze) which are visible from a fire burning in Pike National Forest, Colorado, USA.

SPOT 1, the first French satellite, which was developed with the participation of Sweden and Belgium, was launched in 1986. SPOT 2, 3 and 4 followed in 1990, 1993 and 1998 respectively. SPOT 5 has been launched in Oct, 2001 to ensure continuity of service. The details of bandwidth and resolution are given in Table 1. The viewing angle of each HRV sensor can be adjusted to collect data up to 27 degrees right or left of satellite nadir. This cross-track pointing capability allows the same point on the earth to be viewed from several different orbits and enables the acquisition of stereoscopic imagery (<http://www.SPOTimage.fr>).

Satellites. They orbit the Earth in about 100 minutes and in 35 days, 780 km up and cover nearly every corner of the globe at least once. Both satellites are still in good health and provide a wealth of observations through their excellent suite of instruments. ERS-1's payload consists essentially of two specialized radars plus infrared sensor. The Active Microwave Instrument, the biggest on-board system, produces extremely detailed images. In wind and wave modes, the instrument measures continuously and globally, wind speed and direction together with the ocean wave parameters. It is almost like taking a picture using a flashbulb where the scene is illuminated with radio waves, and the intensity of the returned radio signal gives a record of brightness for each part of the scene. The reflected energy at a given radio wavelength depends primarily on the texture of the surface and on its electrical properties. Since it provides its own illumination of the scene, SAR imaging



Figure 4: LANDSAT image of outer banks of North Carolina, USA, showing after-effects of Hurricane Floyd (source: <http://LANDSAT.gsfc.nasa.gov>)

ERS-1 and ERS-2 are the most sophisticated Earth observation satellites ever developed in Europe (European Space Agency), as a family of multi-disciplinary Earth Observation is referred to as an active form of remote sensing. When two consecutive images are merged through the technique of interferometry, the instrument can even detect landslides and depressions over an approximately 100 x 100 km area. ERS-2, launched in 1995, is a

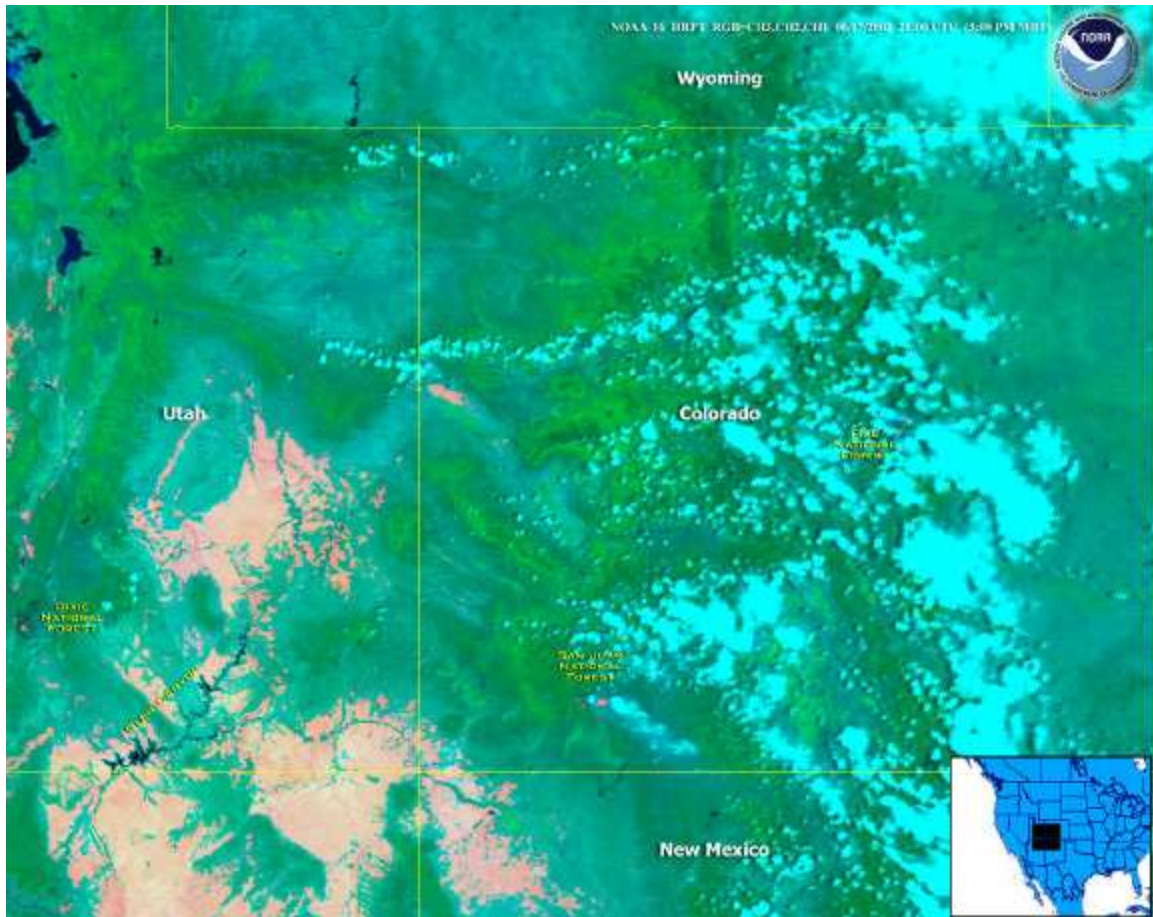


Figure 5: NOAA-AVHRR image showing a fire (red) visible in Pike National Forest, Colorado, USA (source: <http://www.osei.noaa.gov/Events/Fires/>)

carbon copy of ERS-1 with an additional new instrument, Global Ozon Monitoring Experiment (GOME), designed to measure stratospheric and tropospheric ozone (<http://www.deos.tudelft.nl/ers>). Radar imaging uses very short radio waves, in the electromagnetic spectrum, which can pass through few things, like clouds and dry desert sand that block visible light. It is used in tropical areas where continual cloud cover makes visible light imaging difficult and also to discover ancient buried riverbeds that



Figure 6: SPOT image showing oil outflow area of Tokyo Bay taken on July 3, 1997  
(source:[http://www.eoc.nasda.go.jp/guide/topics/news/oil\\_outflow\\_970703\\_e.html](http://www.eoc.nasda.go.jp/guide/topics/news/oil_outflow_970703_e.html))

once held flowing water. Figure 7 is an example of ERS image of volcano eruption in the Vatnajökul glacier. In Figure 7(a), which was captured on 22 October 1996, the water

seems to have frozen and appears calm. In Figure 7(b), taken on 24 October 1996, the SAR is right-looking and this is the first view towards the east. Figure 7(c) has been taken after the eruption (7 November 1996) showing clearly that things have calmed down even if they have not quite returned to normal.

The first MOS (Marine Observation Satellite) – MOS 1 was launched in 1987 and then MOS 1b was put into the orbit in 1990. Funded and managed by the National Space Development Agency of Japan (NASDA), the MOS has a repeat cycle of 17 days. The MOS payload consists of four primary classes of instruments – (i) Two MESSR (Multi-spectral Electronic Self-Scanning Radio-meter), (ii) The Visible and Thermal Infrared Radiometer (VTIR) operates in one visible and three IR bands, (iii) The Microwave Scanning Radiometer (MSR) and (iv) Data Collection System Transponder (DCST). MOS 1 and MOS 1b are expected to remain operational until 2001-2002 (Johnson and Rodvold, 1994; Spaceflight, 1987; NASDA, 1992; Davis, 1993). Figure 8 is an illustration of MOS 1b satellite imagery of Japan Sea surface temperatures.

JERS-1, the Japan Earth Resources Satellite was launched in February 1992, into a 570-km, sun-synchronous orbit (NASDA, 1990), carrying two closely matched Earth observation sensors - the SAR and the OPS multi-spectral imager, comprising of a 3-band, CCD Visible and Near-lit Radiometer (VNIR) and a 4-band, CCD Short Wavelength IR Radiometer (Table 1). The mission of JERS-1 did not last long, but in the end it was possible to obtain observation data of the earth (with regard to resources,

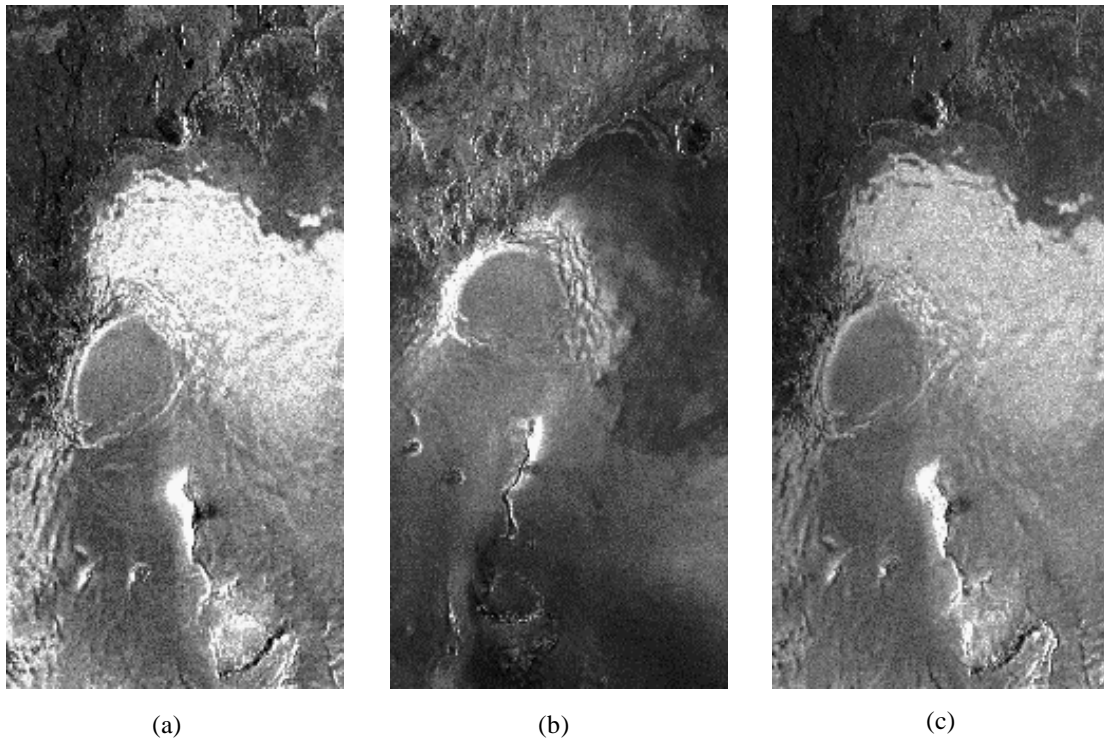


Figure 7: ERS SAR images of 1996 volcanic eruption on the Vatnajökul glacier (source: [http://www.tss.no/gallery/volcano\\_96.html](http://www.tss.no/gallery/volcano_96.html))

disasters and environment, etc) from the satellite for approximately six-and-a-half years (Space News, 1995). Some representative examples of the research results achieved through use of these data are: (a) the retrieval of potential oil mine in Turpan basin of China; (b) the clarifying of the reality of deforestation in the Amazon tropical rainforest; and (c) observation of the of diastrophism (deformation of the earth's crust) caused by the activity of the volcano Mt. Iwateyama (<http://www.fas.org>).



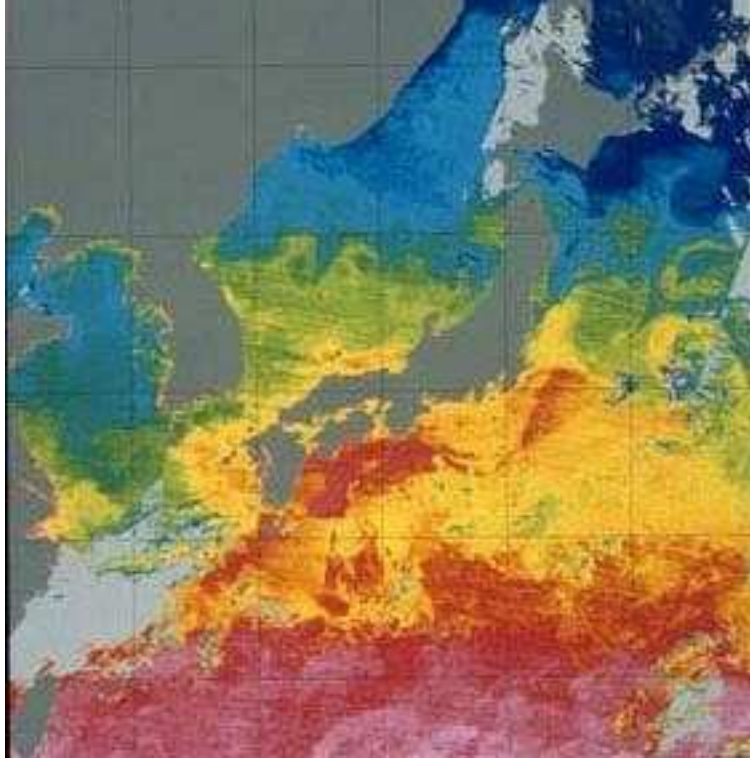


Figure 8: MOS-1 image of sea of Japan taken on May 15-27, 1993, showing sea surface temperature (source: [http://spaceboy.nasda.go.jp/lib/earth/earth/e/earth\\_01\\_e.html](http://spaceboy.nasda.go.jp/lib/earth/earth/e/earth_01_e.html))

IRS (Indian Remote Sensing) series satellites are in the sun-synchronous orbit for more than a decade now. The latest in the series is the second generation IRS-1D, which was launched in 1998 at a mean altitude of 780 km with better resolution, coverage and revisits. It orbits the Earth 358 times in 25 days. The payload has three sensors (Table 1), Panchromatic, Linear Imaging and Self Scanning Sensor (LISS-III) and Wide Field Sensor (WiFS). The satellite is equipped with a 64GB (24minutes) capacity on-board tape recorder, capable of recording limited amount of specified sensor data. Orientation of each of the sensors can be programmed. The PAN payload has a capability to tilt upto an angle of  $\pm 26$  deg, which can be handled with a Payload Steering Mechanism. Figure 9 is an example of IRS-1D satellite's panchromatic 5.8 meter resolution scene.



Figure 9: IRS-1D image showing a panchromatic satellite scene covering Sarajevo airport (source:[http://www.swisstopo.ch/NPOC/Products/kosovo/irsp\\_sarajewo.html](http://www.swisstopo.ch/NPOC/Products/kosovo/irsp_sarajewo.html))

IKONOS satellite ([www.satellus.se](http://www.satellus.se)) has the world's most powerful digital camera system making it the only commercial imaging system for the spaceborne remote sensing. It is designed and built so powerful that it can see objects less than one square meter on the ground and well enough to outline narrow alleys and streets. The satellite will simultaneously collect panchromatic imagery with one-meter resolution, and multispectral data with four-meter resolution, across and 11-km swath of the Earth's surface. The highly detailed topographical images of remote cities and unique geo-information at a very high resolution make IKONOS an important part of disaster mitigation planning and decision-making. Figure 10 illustrates a four-meter resolution

image of Cairo city of Egypt taken on October 21, 1999 featuring Nile River, a suburban area and agricultural fields (<http://www.spaceimaging.com>).



Figure 10: IKONOS four-meter resolution image of Cairo, Egypt  
(source:www.spaceimaging.com)

TSINGHUA 1, the first demonstrator microsatellite for a constellation of seven, to provide daily worldwide high resolution imaging for disaster monitoring and mitigation was launched on 29<sup>th</sup> of June, 2000 ([www.sstl.co.uk/missions/mn\\_TSINGHUA\\_1.html](http://www.sstl.co.uk/missions/mn_TSINGHUA_1.html)). The microsatellite will cost less and will orbit at a lower altitude of 650km. The camera aboard TSINGHUA can image objects up to 39 meters in three spectral bands. But what

makes the microsat test important is how it fits into the next step in the technology program. Sets of five microsats, using the TSINGHUA 1 design, will be orbited as part of a Disaster Monitoring and Mitigation system. TSINGHUA-1 imagery will aid in monitoring vegetation growth in the ambitious large-scale development of the western part of China. Beginning in 2002, the constellation will conduct daily high-resolution imaging of China to track natural and human-made disasters such as wildfires, floods, desertification, and red tides, and assisting farmers in agricultural operations. TSINGHUA 1 can see other satellites too.

Digital Globe launched a low altitude (450km) satellite, QuickBird, on October 18, 2001 opening a new commercial channel with highest publicly available resolution. The satellite has 61cm panchromatic and 2.44 m multispectral sensors. It has stereo capability with 3.5 days revisiting frequency. The sensor can map large areas faster with fewer images, and less ground data to manage and process due to its large swath width of 16.5 km. This would mean that strips of up to 10 scenes in length (165 km) can be collected in a single pass. Areas up to 2x2 scenes can be collected in a single pass. Figure 11 is a QuickBird image example of Tarpani, Sicily captured on February 4, 2002 at spatial resolution of 70 cm.

## **2.2 Various Sensors and Their Applications**

AVHRR sensors (Table 1) on board the NOAA satellites acquire data in three formats – (i) High Resolution Picture Transmission (HRPT), (ii) Local Area Coverage (LAC), and (iii) Global Area Coverage (GAC).



Figure 11: QuickBird image of Tarpani, Sicily captured on February 4, 2002  
(source: <http://www.eurimage.com/gallery/>)

The HRPT, also known as HRV (High Resolution Visible imaging) instrument is a multispectral radiometer designed for SPOT spacecraft. It captures transmissions in the visible and near-infrared portions of the electromagnetic spectrum. The first three SPOT satellites carry twin HRVs that operate in a number of viewing configurations and in different spectral modes. LAC are full resolution data that are recorded on an onboard tape recorder for subsequent transmission during a station overpass. AVHRR data are good for monitoring land/forest fires. In particular, 3.8  $\mu\text{m}$  infrared band is used in hot spot detection (<http://edc.usgs.gov/glis/hyper/guide/avhrr#avhrr14>)

SPOT satellites have the capability of scanning in either a multispectral or a panchromatic mode. Further details of the bandwidths are given in Table 1.

A successful combination of the coverage from two different resolution satellite sensors can work wonders in fire disaster mitigation. It works like this – an agency can download, from the website, the required AVHRR images daily and derive the hotspot images to know the general locations of any fire. SPOT passes of the next day can then be programmed to steer the sensors to zoom in onto the disaster location. If the fires are detected in the SPOT scenes, its passes could be programmed over the areas for the next few days to monitor the development of the fires. With the combination of SPOT-1, 2 and 4 (3 is out of service) any given location can be observed almost daily. The Center for Remote Imaging, Sensing and Processing (CRISP) at the National University of Singapore carries out fire detection on a daily basis, listing the location (longitude and latitude), smoke plume condition (length, width and thickness), wind direction, the type of land cover (forest, plantation, peat swamp, etc.) and the extent of burnt scar associated with each fire (<http://www.crisp.nus.edu.sg>).

TM sensor, on board LANDSAT satellites, collects data in the range of visible (blue), through the mid-IR, into the thermal-IR portion of the electromagnetic spectrum. Sixteen detectors for the visible and mid-IR wavelength bands in the TM sensor provide 16 scan lines on each active scan. Four detectors for the thermal-IR band provide four scan lines on each active scan (Table 1). Capabilities of each band are given on the following

several websites - <http://edcwww.cr.usgs.gov>, <http://ltpwww.gsfc.nasa.gov>, and [www.geoimage.com.au](http://www.geoimage.com.au).

SAR imaging systems (on-board RADARSAT, ERS and JERS) are capable of collecting images using advanced microwave techniques to make measurements and acquire imagery regardless of atmospheric or sunlight conditions and under most weather conditions, which makes this data ideal for use in mapping projects where persistent cloud cover or darkness impede acquisition by optical imaging systems. The C-band wavelength responds to different aspects including gross surface roughness, moisture content and dielectric properties (pertaining to non-conductors of direct electric current) and therefore, forest fire detection, flood delineation and forest monitoring (due to backscatter intensity and interferometric coherence). The detailed account of payload of instruments on-board ERS is available on the following websites - [www.crisp.nus.edu.sg](http://www.crisp.nus.edu.sg), and [www.deos.tudelft.nl](http://www.deos.tudelft.nl).

Two MESSR (Multi-spectral Electronic Self-Scanning Radio-meters) in MOS return images in four bands (Table 1) with a ground resolution of 50 m and a swath of 100 km. The fields-of-view of the two MESSR sensors are slightly overlapped (15 km) to provide stereo viewing. This sensor's main objectives are to capture air and sea related information. The Visible and Thermal Infrared Radiometer (VTIR), good for clouds and temperature of ocean surface. The Microwave Scanning Radiometer (MSR) is useful for sea surface, water vapor, snowfall and desertification. Finally, the Data Collection System Transponder (DCST) collects data from DCP's transmitting in the 400 MHz band

and relays the information to data acquisition and processing ([www.eoc.nasda.go.jp](http://www.eoc.nasda.go.jp) and [www.fas.org](http://www.fas.org)). Figure 12 shows Mt. Aso in Japan, which was very active during Jun/89-Feb/91 in the term of MOS observation. Especially, in the autumn of 1989, heavy ash-falls gave serious damages to the agriculture and traffic inside the caldera and its neighboring regions.



Figure 12: MOS – MESSR image of ash cloud on October 18, 1989  
([http://www-sci.edu.kagoshima-u.ac.jp/sing/image/A/aso\\_unzen/m89a-aso-e.htm](http://www-sci.edu.kagoshima-u.ac.jp/sing/image/A/aso_unzen/m89a-aso-e.htm)).

LISS-III, which is on-board IRS-1D, operates in four bands in visible, near infrared and short wave regions. Since the first three bands are in the same spectral region as the previous launches IRS-1A/1B/P2 sensors, the continuity of data received is maintained (Table 1). Sensors in IKONOS are panchromatic and multispectral, capturing data in the



spectral band of VNIR (visible and near infrared). The satellite can revisit an area in 2.9 days at 1-meter resolution and 1.5 days at 1.5-meter resolution. These values are for targets at 40 degrees latitude. The revisit times will be more frequent for higher latitudes and less frequent for latitudes closer to the equator.



Figure 13: IRS-1C LISS image of Sarajevo airport captured on August, 24, 1998 (source: [http://www.swisstopo.ch/NPOC/Products/kosovo/irsli\\_sarajewo.html](http://www.swisstopo.ch/NPOC/Products/kosovo/irsli_sarajewo.html))

### **3. DISASTER MANAGEMENT AND REMOTE SENSING**

Since the first Earth Resource satellite, LANDSAT-1, was launched in 1972, we have come a long way in terms of improved sensors with better spatial and temporal

resolutions. Different satellites and sensors can provide unique information about properties of the surface or shallow layers (top soil layer) of the Earth. For example, measurements of the reflected solar radiation give information on albedo, thermal sensors measure surface temperature, and microwave sensors measure the dielectric properties and hence, the moisture content, of surface soil (Portmann and Mendel, 1997, Rombach and Mauser, 1997) or of snow.

The impact of natural disasters can be reduced through a proper disaster management, including disaster prevention (hazard and risk assessment, land use planning and legislation, building codes), disaster preparedness (forecasts, warning, prediction) and rapid and adequate disaster relief (OAS, 1990; UNDRO, 1991). Mitigation of natural disasters can be successful only when adequate knowledge is obtained about the expected frequency, character, and magnitude of hazardous events. Some types of disasters, like, floods or earthquakes may originate very rapidly and may affect large areas. The use of synoptic earth observation methods has proven to be especially suitable in the field of disaster management. In a number of countries, where warning systems and building codes are more advanced, remote sensing of the earth has been found successful to predict the occurrence of disastrous phenomena and to warn people on time.

About 95 % of the natural disaster related deaths occur in the developing world, where more than 4200 million people live. Economic losses attributable to natural hazards in developing countries may represent as much as 80% of their gross national product. In India for example natural catastrophes have taken the lives of 1.6 million people since

1960, and caused over 16 billion US\$ losses (Munich Reinsurance Company, 1998), mainly due to drought, famine, tropical cyclones, floods and earthquakes. However, disasters are not inevitable all over the world (Dutta and Herath, 1999).

In this review work the authors have discussed the following few forms of natural hazards: earthquakes, volcanic eruptions, tsunamis, hurricanes, landslides and floods.

### **3.1 Earthquakes**

The earthquakes can occur in cycles of decades or centuries. Scientists of the U.S. Geological Survey (USGS) have operated seismographic stations throughout the world for more than 35 years. For the past few years, in cooperation with the Incorporated Research Institutions for Seismology (IRIS - a consortium of more than 90 universities), the USGS has upgraded the system into a state-of-the-art Global Seismographic Network (GSN). The GSN is designed for obtaining high quality data in digital form that can be readily accessed by data users worldwide. For some stations, the data is reported to orbiting satellites, and then to the Internet where information can be viewed using the World Wide Web.

Remote sensing techniques can add-up to the information available through seismic techniques. Generally, the faults associated with earthquakes can be identified on good resolution satellite imagery, whereas the volcanic related earthquakes are not all that obvious (Richards, 1982). For this purpose land use and geological maps can give vital pointers towards potential earthquake zones. Satellite sensors that are active in the visible

and near infrared spectral band would be useful. Though IRS (IRS-1D Handbook, 1997), NOAA ([www.usgs.gov](http://www.usgs.gov)), SPOT ([www.SPOTimage.fr](http://www.SPOTimage.fr)), LANDSAT ([www.nasa.gov](http://www.nasa.gov)) and IKONOS ([www.spaceimaging.com](http://www.spaceimaging.com)) all of them collect the required data, LANDSAT imageries are more popular because of the long historical data archives of the satellite and its cost effectiveness. Conventionally, aerial remote sensing (airborne radar) would be thought as more effective to delineate unconsolidated deposits sitting on fault zones, upon which most of the destruction occurs, and to identify areas where an earthquake can trigger landslides but now with 1m resolution satellite imageries professionals are very hopeful to apply more and more of remote sensing techniques.

Figure 14 is an illustration of earthquake imagery in which one-meter resolution image, taken by Space Imaging's IKONOS satellite on February 2, 2001 shows the town of Bhuj, located in the northwestern state of Gujarat, India. The image shows extensive damage to individual buildings as a result of the earthquake that struck Bhuj on January 26, 2001. While many buildings suffered structural damage, such as cracked walls, the IKONOS satellite can only detect buildings that have fully collapsed with altered rooflines. This type of imagery could be used to assist authorities with immediate mitigation activities such as search and rescue efforts, emergency relief and major infrastructure damage assessment.

### **3.2 Volcanic Eruptions**

There are some 500 active volcanoes around the globe, about 100 of which erupt every year ([www.SPOTimage.fr](http://www.SPOTimage.fr)). Volcano monitoring is important simply because an unexpect-



Figure 14: Earthquake in Bhuj, India captured by IKONOS on February 2, 2001 (source: <http://www.spaceimaging.com/carterra/applications/disaster/mozambique.htm>)

ted awakening can imperil thousands of lives over a wide area. Remote sensing techniques can play an important role by providing the vital information with only limited fieldwork, which saves effort and money.

Thermal infrared (TIR) imagery can capture the volcanic heat provided the spatial resolution is high enough. Also, PAN stereo-pair imagery, due to its 3-D capabilities, of moderate resolution would serve the purpose of finding out the evidence of hazardous activities. An IR pattern of geothermal heat in the vicinity of a volcano is an indication of thermal activity, which many inactive volcanoes display. Many volcanoes thought to be extinct may have to be reclassified if regular monitoring discovered any abnormally

high IR emissions from either the summit craters or the flanks. Changes in thermal patterns can be obtained for a volcano only through periodic IR imageries of very high resolution, like that of IKONOS, taken under similar conditions of data acquisition. The temperature and gas emission changes, however, can be monitored, through a geostationary satellite, at ideal locations identified on the thermal imagery.

The TIR bands of AVHRR sensor on NOAA satellite can detect volcanic ash as it has a strong signal difference between channel 4 and channel 5 (Table 1). The spatial resolution of AVHRR may not be adequate to detect the dynamic change in volcanic geothermal activity in some situations. In a case study conducted by Petkov et al (1996), satellite thermal estimates from six scenes were first compared to ground measurements of maximum daily temperature. The results show that the estimated model parameters from the various methods are quite different and the fitting of the experimental points to the theoretical model is much better when using continuous satellite data. This finding has interesting implications for the more general problem of defining standard optimum interpolation methods, which would ultimately help in volcano monitoring methodology.

LANDSAT, SPOT-4 and IRS-1D imagery is a valuable aid in detecting the volcanic activity. The SWIR band in particular is well suited for locating fire hot SPOTs, lava flows and intense volcanic activity. Once alerted by early-warning systems, specialists need to monitor levels of volcanic activity continuously so that timely precautions can be taken. The level of energy detected is the sum of reflected and emitted energy. The energy emitted by lava makes it visible in the NIR band but not in the red band.

However, the fact that hot SPOTs are equally well detected at night shows that reflected energy only accounts for a small portion of the total energy measured. This property proves useful in determining the temperature of hot SPOTs, lava flows and intense volcanic activity. Imaging sensors can detect hot SPOT because they measure the energy emitted from surfaces at temperatures of 220° to 520°C. Though vulcanologists rely widely on LANDSAT imagery to obtain this kind of information, SPOT's resolution and radiometric sensitivity can detect a wider range of temperatures, while its frequent revisit capability enables truly operational monitoring of a region of interest. Figure 15 is a set of six images showing the Crater of Piton de La Fournaise volcano, Réunion Island, in the western Indian Ocean, which is a particularly good illustration. A survey carried out between 7 June and 13 July 1998 using eight scenes acquired by SPOT 4 was able to monitor rapid variations in volcanic activity.

Oppenheimer (1997) has shown that water surface temperature and area can be measured simultaneously by using all seven spectral bands of LANDSAT Thematic Mapper (TM). Crater lakes on active volcanoes act as heat and chemical traps, and are amenable to surveillance from space. The case studies on several volcanoes, namely, Ruapehu (New Zealand), Taal (Philippines), Kawah Ijen and Kelut (Indonesia), Poas (Costa Rica), Apoyeque and Jiloa (Nicaragua) indicate that lake surface temperatures derived by TM band 6 are typically 1 - 4 degrees less than contemporaneously measured bulk temperatures. This is a small difference compared to the magnitude of volcanogenic changes in lake temperature and do not reduce the utility of IR surveillance. Also, TM-derived water surface spectral reflectance indicates high concentrations of suspended chemical sediment in the most active crater lakes, viz., Ruapehu, Poas and Ijen. The

Advanced Spaceborne Thermal Emission and Reflectance Radiometer (ASTER) and Enhanced Thematic Mapper (ETM), already launched in 1998 might prove to be better for remote surveillance of crater lakes.

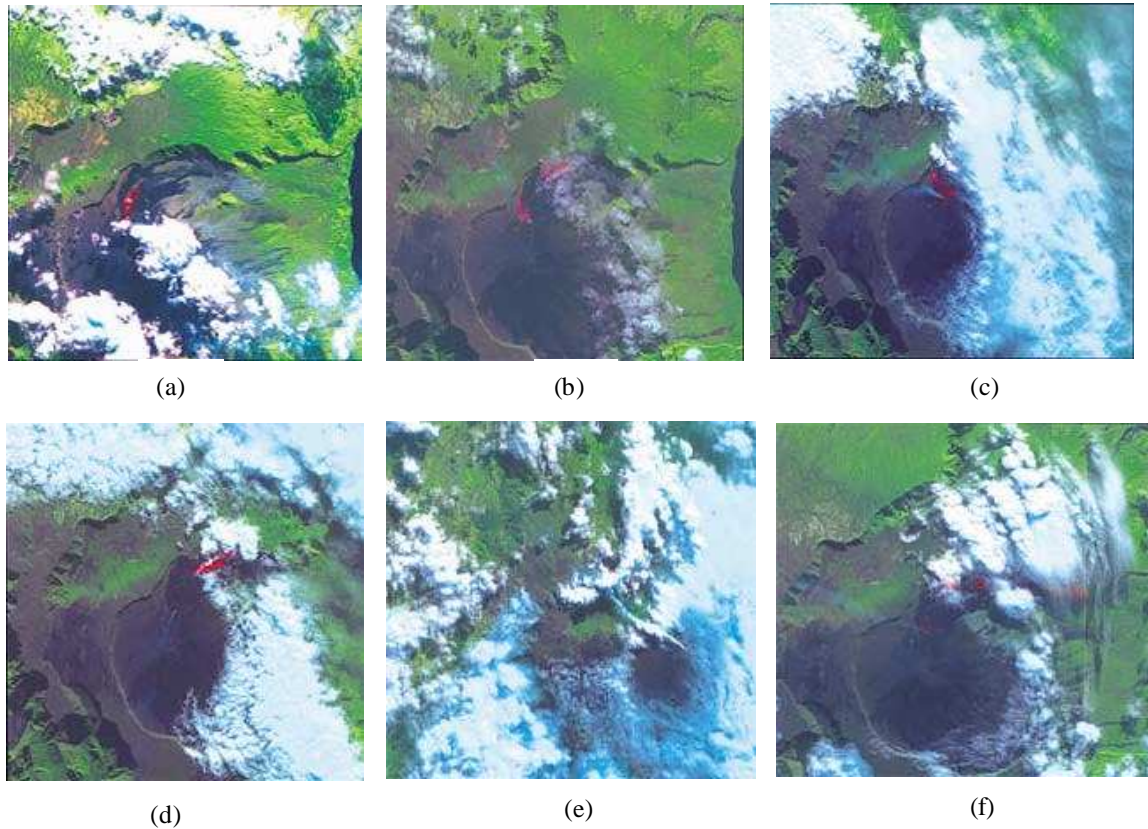


Figure 15: Volcanic eruption - from top left (a) June 7: lava can be seen flowing north-west, (b, c) June 22 and 23: smoke is venting from the volcano and the lava flow is moving north, (d) July 2: the eruption is still visible despite thick cloud cover, (e) June 28: the lava flow is very wide. The yellow line in the center of the lava stream indicates temperatures close to  $1000^{\circ}$ , (f) July 8: the lava flow has advance considerably eastward and is threatening to reach the coast road.

A particularly good illustration is a survey, carried out, in the western Indian Ocean, between 7 June and 13 July 1998 using eight scenes acquired by SPOT. Vulcanologists



were able to monitor rapid variations in volcanic activity (Lardy and Sigaud, 1995) when the volcanoes entered a dangerously active phase. The repeat feature of SPOT can closely monitor (e.g., the Piton de La Fournaise volcano) the lava flow. Another volcano, Lombenden, which is one of the world's few active volcanoes with a hot acid crater lake, in the Vanuatu archipelago in the southwest Pacific was studied by the French scientific research organization, ORSTOM. Lombenden appears to have become more active since 1991 as revealed by tree dieback on the islets and around the shores of Lake Vouli and also could be seen in a SPOT scene acquired in 1992. The image, taken 17 days after the explosion revealed that the level of the lake is about 6m lower than before. Variations in the temperature and chemical composition of crater lakes reveal changes in volcanic activity. The area of each lake and the areas where all or a large proportion of trees had been killed by volcanic gases can be calculated, allowing us to identify the zone affected by gas dissolution. The study was able to develop and test a methodology for monitoring volcanoes that is reliable, offers high performance, and enables vulcanologists to significantly reduce the amount of field work.

### **3.3 Tsunamis**

Tsunamis are water waves or seismic sea waves caused by large-scale sudden movement of the sea floor (due to earthquakes; landslides; volcanic eruptions or man-made explosions). With increasing population and development along most coastlines, there is a corresponding increase in tsunami disaster risk in recent years. Tsunamis differ from other earthquake hazards in that they can cause serious damage thousands of kilometers from the causative faults. Once they are generated, they are nearly imperceptible in mid-

ocean, where their surface height is less than a meter. They travel at incredible speeds, as much as 900 km/hr, and the distance between wave crests can be as much as 500 km. As the waves approach shallow water, a tsunami's speed decreases and the energy is transformed into wave height, sometimes reaching as high as 25 m, but the interval of time between successive waves remains unchanged, usually between 20 and 40 minutes. When tsunamis near the coastline, the sea recedes, often to levels much lower than low tide, and then rises as a giant wave.

The Pacific Tsunami Warning Center (PTWC) provides warnings for Pacific basin teletsunamis (tsunamis that can cause damage far away from their source) to almost every country around the Pacific rim and to most of the Pacific island states. Satellite or aerial photography, especially when combined with a good GIS database of an area, can provide critical information for emergency managers, including damage to structures, transportation and communication links, and other "life-line" infrastructure components. Figure 16 is a set of two air photos taken before (left) and after (right) a tsunami struck Okushiri Island, Japan, on 12 July 1993, killing more than 200 persons.

### **3.4 Hurricanes**

These large-scale low-pressure systems occur throughout the world over zones referred to as "tropical cyclone basins" ([www.oas.org/usde/](http://www.oas.org/usde/)). The determination of past hurricane paths for the region can be derived from remotely sensed data from the U.S. National Oceanographic and Atmospheric Administration (NOAA) satellite sensors designed and operated for meteorological purposes. The Tropical Analysis and Forecast Branch of the



Figure 16: Aerial photo of before and after tsunami hit an area (source: [http://www.pmel.noaa.gov/tsunami/aerial\\_photo\\_okushiri.html](http://www.pmel.noaa.gov/tsunami/aerial_photo_okushiri.html))

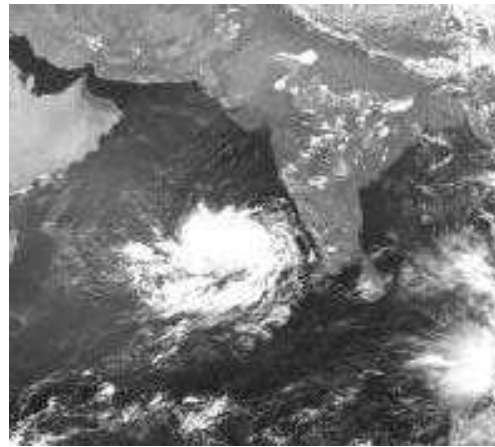
Tropical Prediction Center (TPC) provides year-round products involving marine forecasts, aviation forecasts and warnings (SIGMETs), and surface analyses. The unit also provides satellite interpretation and satellite rainfall estimates for the international community. The Technical Support Branch provides support for satellite data processing. One of the key lessons NASA learned during Hurricane Andrew was that it is critical to select appropriate data and put it together to make informed decisions. Due to the lengthy process required to gather the data, it was suggested that communities not wait until a disaster happens to do so. Imagery is an important aspect of a community's database. The next generation of satellites such as Earthwatch's Early Birds and Astrovision will significantly enhance the remote sensing capabilities. At present, for plotting new data, the best sensor is the AVHRR with its 2,940 km swath, twice-a-day coverage and appropriate resolution. The red band is useful for defining daytime clouds and vegetation,

while the TIR band is useful for both daytime and nighttime cloud observations. Figure 17 shows a NASA GOES image of hurricane Bret that hit Texas on August 22, 1999.

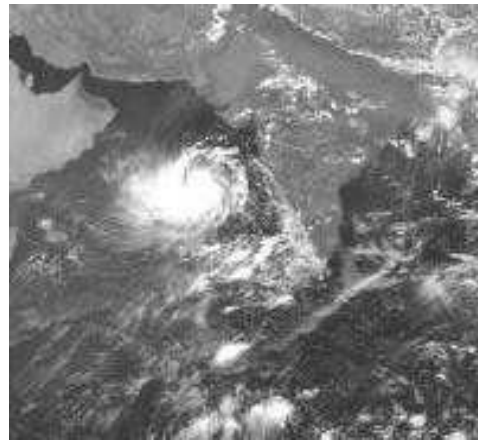


Figure 17: Hurricane Bret that hit Texas on August 22, 1999 (source: <http://rsd.gsfc.nasa.gov/pub/goes/990822.bret.jpg>)

METEOSAT-5 observed the development of a destructive cyclone in the Indian Ocean between 5 and 9 June 1998 which was reported to have caused the death of more than 1000 people in India. Figure 18 is a set of four images showing the development of this cyclone.



June 5, 1998



June 7, 1998



June 8, 1998



June 9, 1998

Figure 18: Development of a cyclone in the Indian Ocean captured by METEOSAT-5 between 5 and 9 June 1998 (source: <http://www.eumetsat.de/en/>)

### 3.5 Landslides

An area with a potential landslide hazard usually has some evidence of previous occurrences. An examination of stream traces frequently shows deflections of the bed course due to landslides. Typical features that signify the occurrence of landslides

include, chaotic blocks of bedrock whose only source appears to be upslope, crescentic scarps or scars whose horns point downward on a normal-looking slope, abnormal bulges with disturbed vegetation at the base of the slope, large intact beds of competent sedimentary or other layered rock displaced down dip with no obvious tectonic relationship and mudflow tongues stretching outward from the base of an obviously eroded scar of relatively unconsolidated material ([www.oas.org/usde/publications/](http://www.oas.org/usde/publications/)).

The spatial resolution required for the recognition of most landslide features is about 10 m (Richards, 1982). However, the recognition depends to a great extent on the ability and experience of the interpreter and is enhanced by the availability of stereoscopic coverage, which can be expensive to acquire. Although large block landslides can be detected on LANDSAT MSS and TM imagery, SPOT PAN imagery could be preferred with its 10 m resolution or IKONOS 4 m multispectral image would still be better. Thermal IR scanner is particularly useful during the night, due to the maximum temperature difference between the terrain and the ground water, in locating seepage areas that lubricate slides. However, limitations like, low altitude required for reasonable spatial resolution, the large number of flight lines required for the large area involved, and the geometrical distortions inherent in the system restrict the use of thermal IR scanner. X-band SAR can be marginally useful in a stereo mode because of its ability to define some larger textures related to landslides. In some cloud-prone environments SAR may be the only sensor that can provide interpretable information.

Metternicht and Zinck (1998) successfully demonstrated that LANDSAT TM and JERS SAR data covering the VIS, IR, thermal and microwave regions of the spectrum could be implemented to detect and map soil erosion features in the Sacaba Valley in Bolivia. The synergy of LANDSAT TM and JERS SAR data provided a unique combination that allowed more accurate identification of bad lands, slightly eroded areas, miscellaneous land, fallow land and moderately eroded areas, as compared to the results obtained by LANDSAT TM alone. Accurate land use classification is important if our aim is to assess the damages due to any natural disaster. Stussi et al (1996) and Liew et al (1999) have examined the use of SAR Interferometry (INSAR) data for classification between vegetated and non-vegetated areas and monitoring vegetation respectively, for, it is well known that forest greatly affects the coherence of radar backscatter. The coherent condition of the signals received by two spatially displaced antennas, which forms the basis of what is now called SAR Interferometry, provides useful information about the topography of the terrain.

Oštir et al., have also presented, in their study, the use of various satellites (ERS, SPOT, RADARSAT and LANDSAT) imagery to study the impact and damages due to the landslide that occurred in Mangart stream ravine situated under Mount Mangart ridge, near Bovec in the north-western part of Slovenia. Figures 19(a), state before, and 19(b), state after were used to estimate the total damage and impact of the landslide.

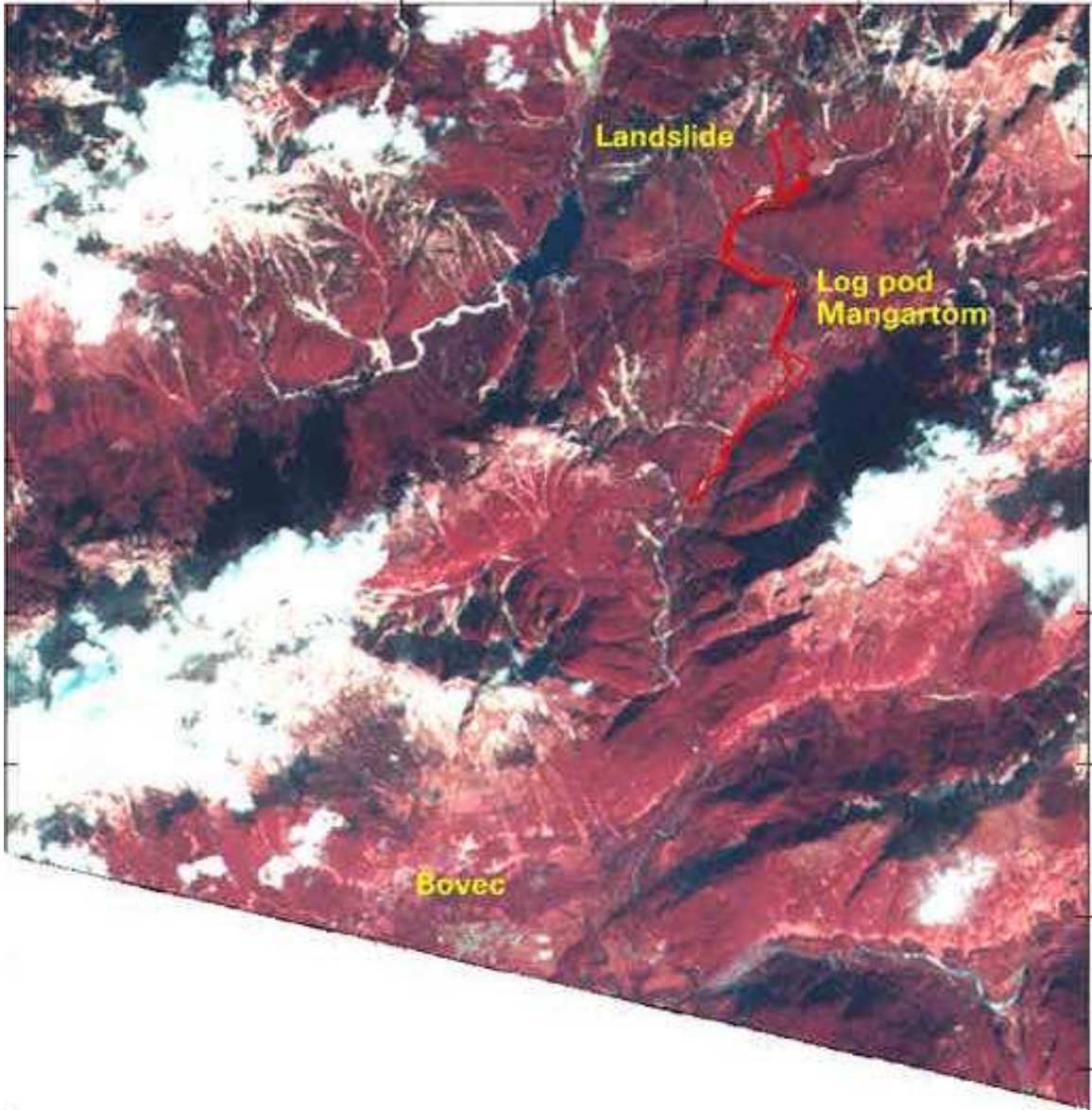


Figure 19 (a): SPOT multispectral images acquired before landslide on August 19, 2000





Figure 19 (b): SPOT multispectral image acquired after a landslide on 29 November 2000

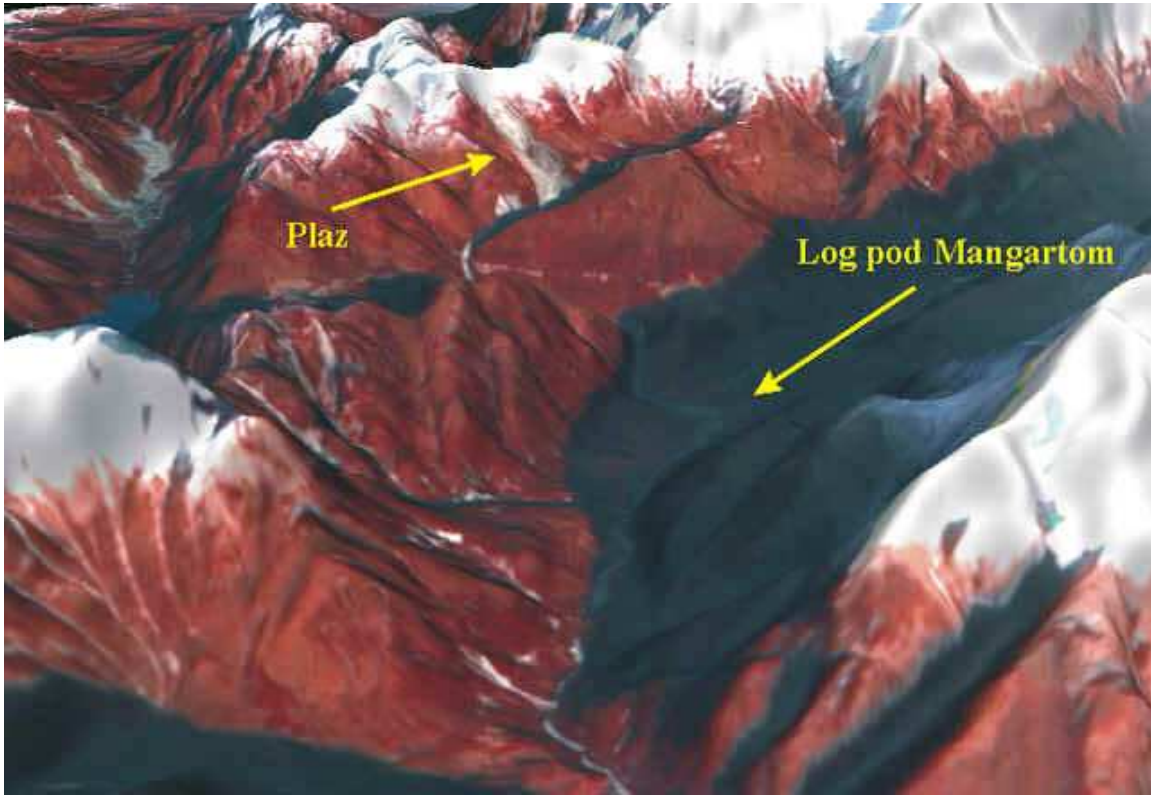


Figure 19 (c): Perspective view of the area -A merged SPOT pan-multispectral image is draped over a DEM (source: <http://www.zrc-sazu.si/pic/pub/log/log.htm>)

### 3.6 Floods

According to the Federal Emergency Management Agency (FEMA) of the USA, floods are the second most common and widespread of all natural disasters. Within the USA an average of more than 225 people are killed and more than \$3.5 billion in property is damaged by heavy rain and flooding each year (<http://www.fema.gov/library>). Scientists and researchers have been investing valuable hours and funds in finding out more accurate and faster methodologies to predict and estimate flood depth and extent. Satellite imagery can be very effective for flood management in the following way:

- Detailed mapping that is required for the production of hazard assessment maps and for input to various types of hydrological models;
- Developing a larger scale view of the general flood situation within a river catchment or coastal belt with the aim of identifying areas at greatest risk and in the need of immediate assistance; and
- Monitoring land use/cover changes over the years to quantify prominent changes in land use/cover in general and extent of impervious area in particular.

Floods are result of excess runoff, which could increase or decrease depending on various factors, such as, intensity of rainfall, snow melt, soil type, soil moisture conditions and land use and land cover. Runoff from rural and urban areas is generally a response of excess water after the processes of infiltration and evapotranspiration have taken place. Obviously, urban regions will have more of impervious land where infiltration cannot occur. On the other hand rural drainage area will have some water absorbed in the soil till it reaches saturation level sending the rest to contribute to direct runoff. Soil erosion, too, is greatly controlled by vegetation. Dense vegetation provides vegetal retarder to overland flow (Bruynzeel, 1990). Hence, land use classes, as determined by remote sensing, have an implicit hydrological significance in terms of water yield, peak flows and soil erosion (Gorte, 2000). Continuing deforestation leads to more sediment yield downstream causing damages in flood plain agricultural fields (Meijerink and Maathuis, 1997). Since, sudden increase in river flows might also cause floods, the stakeholders

here are not only the watershed management agencies and people living in the region but also insurance agencies who provide insurance against flood damages.

Generally, flood planes and flood prone areas can be identified on remotely sensed imagery (Brakenridge et al, 1998). Two types of efforts have been made in this area – (i) flood mapping (Barber et al, 1996; Okamoto et al, 1998; Saatchi et al, 2000) using images of peak flood/post-flood (with water levels clearly visible) and (ii) flood forecasting, mainly based on clouds patterns (Pankiewicz, 1997; Feidas et al, 2000). For mapping purposes a pre-flood scene and a peak flood image would be compared to delineate the inundated area and based on the land use classification the damages in terms of properties and crops (Stussi et al, 1996; Riley et al, 1997; Liew et al, 1999). One major hurdle in recoding of floods is that clouds are usually present in the atmosphere when rain occurs and therefore, both, LANDSAT and SPOT data would be useful only under cloud-free situations. SAR, which is onboard ERS and RADARSAT satellites, can provide images during the day or night, despite any presence of haze, light rain, snow, clouds or smoke. Therefore, it is most suitable tool for flood inundation mapping and monitoring in a humid temperate climatic environments. Open water surfaces, near-surface moisture, soil moisture changes and the extent of wet snow packs can also be detected by SAR. This sensor is useful in distinguishing between wet snow and dry snow and between wet ground and dry ground. Using suitable images it is possible to create a series of snow cover maps over the period of the snowmelt season to roughly quantify rate of snowmelt in the catchment (Hillard et al, 1999).

An image taken after the flood has receded is useful in assessing damage to buildings and infrastructure. Post-flood image could be an effective tool to evaluate impact of flooding on environmental concerns, such as, coastlines, forests, open space. Figure 20 is an image of Yangtse River in China (during 1998 flood) captured by ERS-1 SAR in June 1998 joined with an ERS-2 SAR image taken on August 1, 1998, providing a multitemporal or change detection rendition. Both blue and red associate with floodwaters.

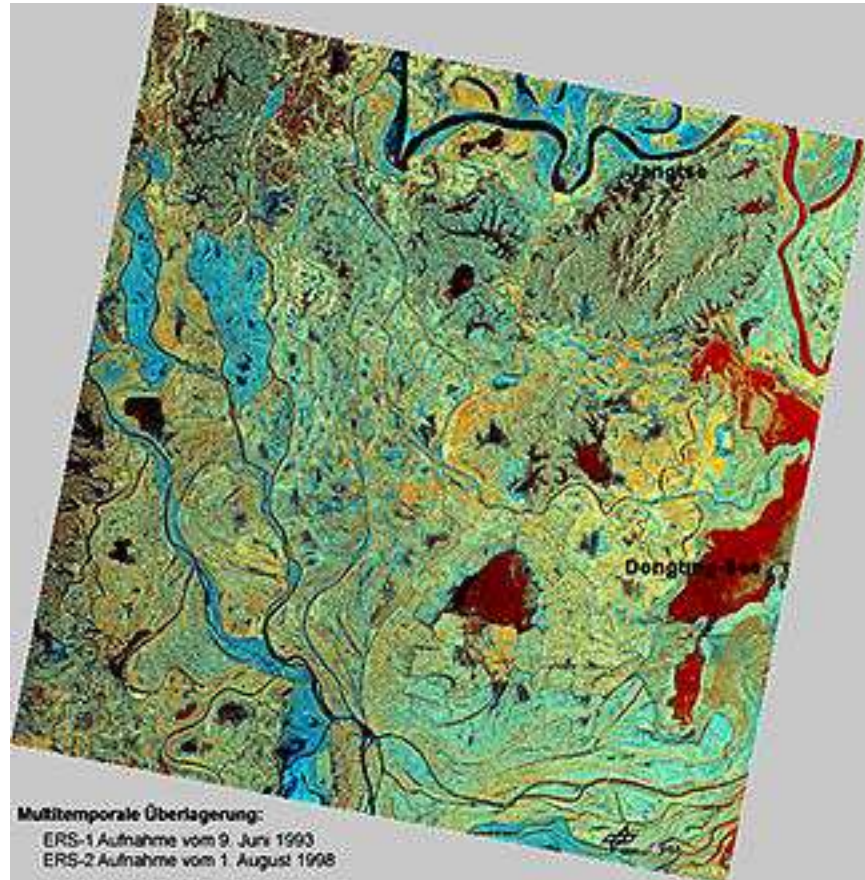


Figure 20: Combination of ERS-1 (June 1998) and ERS-2 (August 1998) SAR imagery of Yangtse River in China (source: <http://www.fas.org/irp/imint/docs/rst/Sect14/>)

### **3.6.1 Flood Mapping**

Conventionally, flood mapping is done by overlaying a pre-flood image and a peak flood image to delineate the inundated area. Damages, in terms of properties and crops, are assessed with the help of existing land use base map (Colby et al, 1999; Brakenridge et al, 1998; Nico et al 2000; Saders and Tabuchi, 2000). Recently, Nico et al (2000) employed amplitude change detection method to detect flood-inundated area using multipass SAR data. However, both the above-mentioned methods allow flooded zones to be identified only when they are flooded at the time of the second satellite pass, and not at the time of the first one. Coherence (two waves are said to be in coherence if their crests and troughs meet at the same place at the same time) derived from multipass interferometry data can be used instead, as an indicator of changes in the electromagnetic scattering behavior of the surface, thus potentially revealing all the area affected by the flood event at any time between the two passes.

In late March of 1973 the Mississippi River in the US experienced a 100-year flood (largest expected statistically in a 100-yr) as a consequence of rapid snow melt and heavy rain. Figure 21 is a LANDSAT-1 image, with an earlier pre-flood view on the left and the extent of flooding on a cloud free day on the right.

Twenty years later the great Mississippi Flood occurred again and damaged 11,000,000 acres of farms, communities, roads and rail links; killing more than 50 people; dislocating millions, some permanently; costing, in federal funds alone, more than \$12 billion

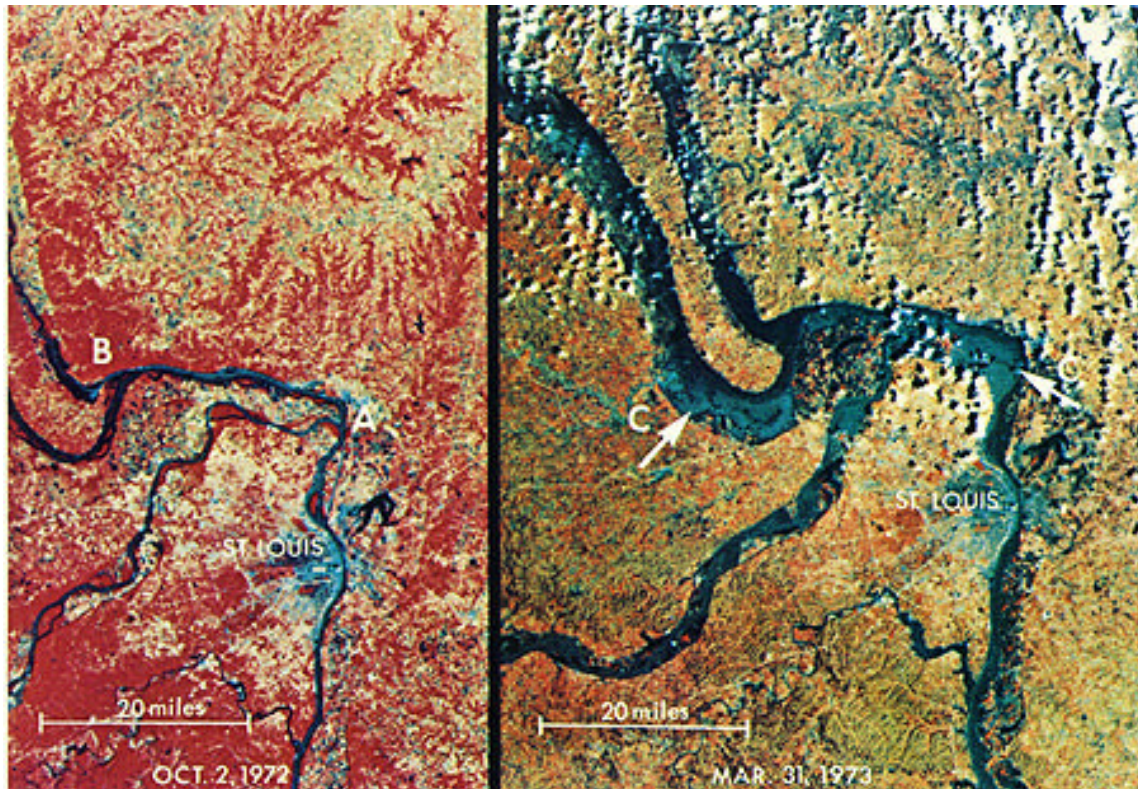


Figure 21: LANDSAT-1 image of March 1973 Mississippi River flood (source: <http://www.fas.org/irp/imint/docs/rst/Sect14/>)

(<http://www.EARTHSAT.com/flood/sast/sast2.html>). Use of hydrologic modeling along with remote sensing data and GIS techniques were applied to work out solutions to mitigate future damages and costs to the federal government. Aerial extent of the flooding was necessary as baseline information for validating flood insurance claims. SPOT PAN image, shown in Figure 22, acquired by EARTHSAT on July 18, 1993 illustrates the sharper definition of features at 10 meter resolution and when focused on West Alton (Figure 23), identification of individual houses was possible.



Figure 22: SPOT PAN image acquired on July 18, 1993 – 10 meter resolution (source: [http://www.earthsat.com/wx/flooding/flood\\_93.html](http://www.earthsat.com/wx/flooding/flood_93.html))





Figure 23: SPOT PAN image focused on West Alton at 10 meter resolution(source: [http://www.earthsat.com/wx/flooding/flood\\_93.html](http://www.earthsat.com/wx/flooding/flood_93.html))

In a mapping study during the 1994 flood in Albany, Georgia, the Army Corps of Engineers (COE) acquired a SPOT PAN image prior to flood and overlaid the county boundaries and the city limits onto the image to map the extent of damages in terms of

people affected and potential cost. The objective of the study was to provide to US Federal Emergency Management Agency (FEMA) a congressional briefing graphic, which would show both flood extent, and the nature of the impacted landscape.

The flood prone coastal plain of Texas got flooded after a heavy precipitation in the autumn of 1994. So, to detect, measure, and display the geographic extent of newly urbanized areas, SPOT PAN images were used. This turned out to be a cost effective procedure for evaluating expanding urbanization and its relationship to floodplains and flood risk. The information is useful for the risk insurance agencies as well. High risk areas that need visual inspection can be identified using the land use change information in the form of a map.

Red River flood in 1990 was one of the larger floods in Canada and south of the boarder. Three images in Figure 24 were captured by SPOT before the flood in 1987 (top image), during the flood in 1990 (middle image) and flood inundated area during the flood (bottom image). Barber et. al. (1996) demonstrated how ERS SAR and LANDSAT TM can be used in both the assessment and mitigation components of flood management. They discovered that high incidence angle SAR at 5.3 GHz and HH polarization is ideal for delineating flood boundaries. TM data integrated with SAR is found to be ideal for efficient computation of total flooded area, flooded area by land use class, and spatial association of these variables with other demographic, socio-economic, or cultural variables.

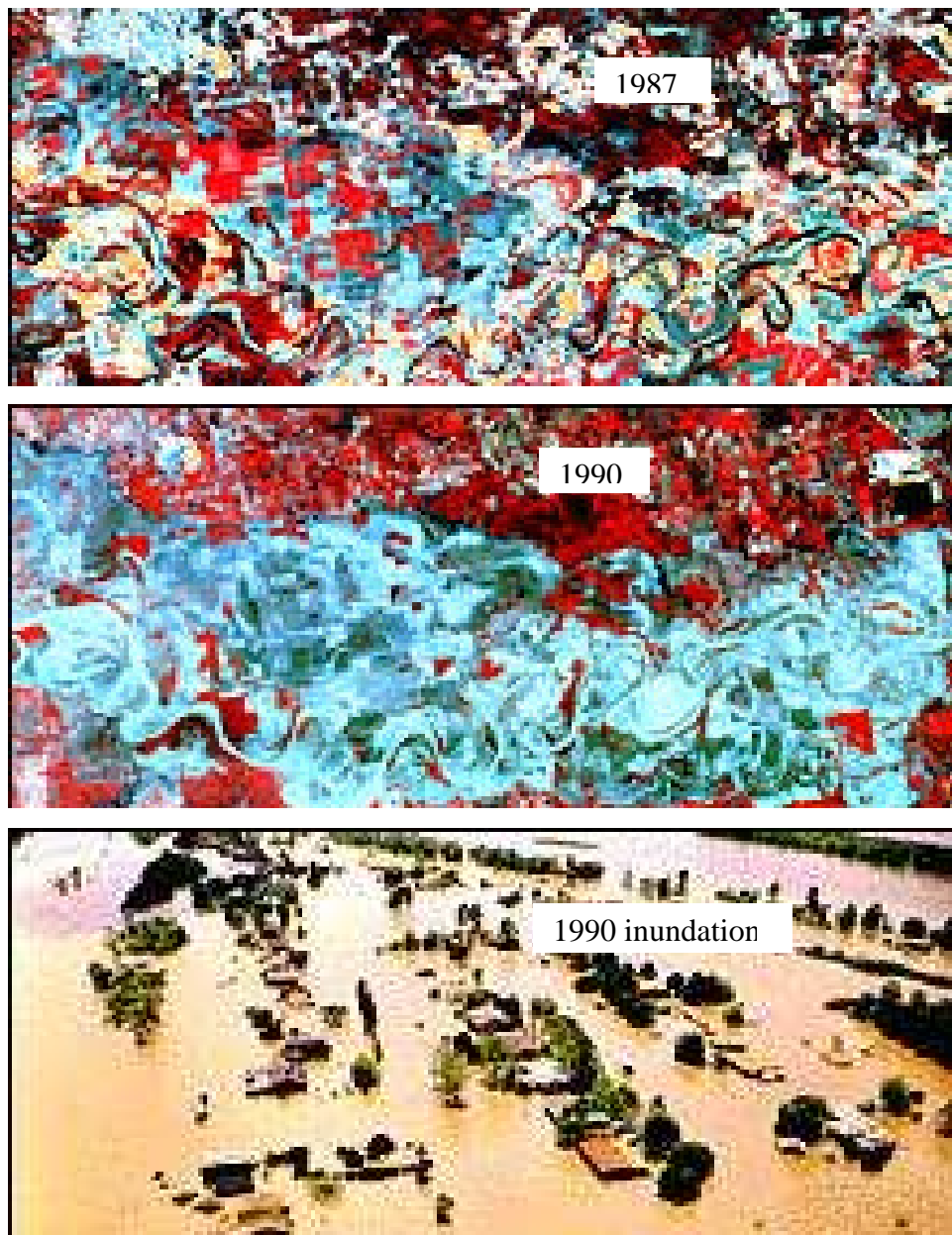


Figure 24: SPOT image of 1990 flood of Red River  
(source:<http://www.spotimage.fr/home/appli/hazard/rriver/welcome.htm>)

Figure 25 is the examples of Landsat imagery captured on May 11, 1997 of the Red River flooding in Manitoba, Canada. These images greatly helped the professionals in mapping the high and low risk areas and in assessing the damages to the properties in flood affected region.

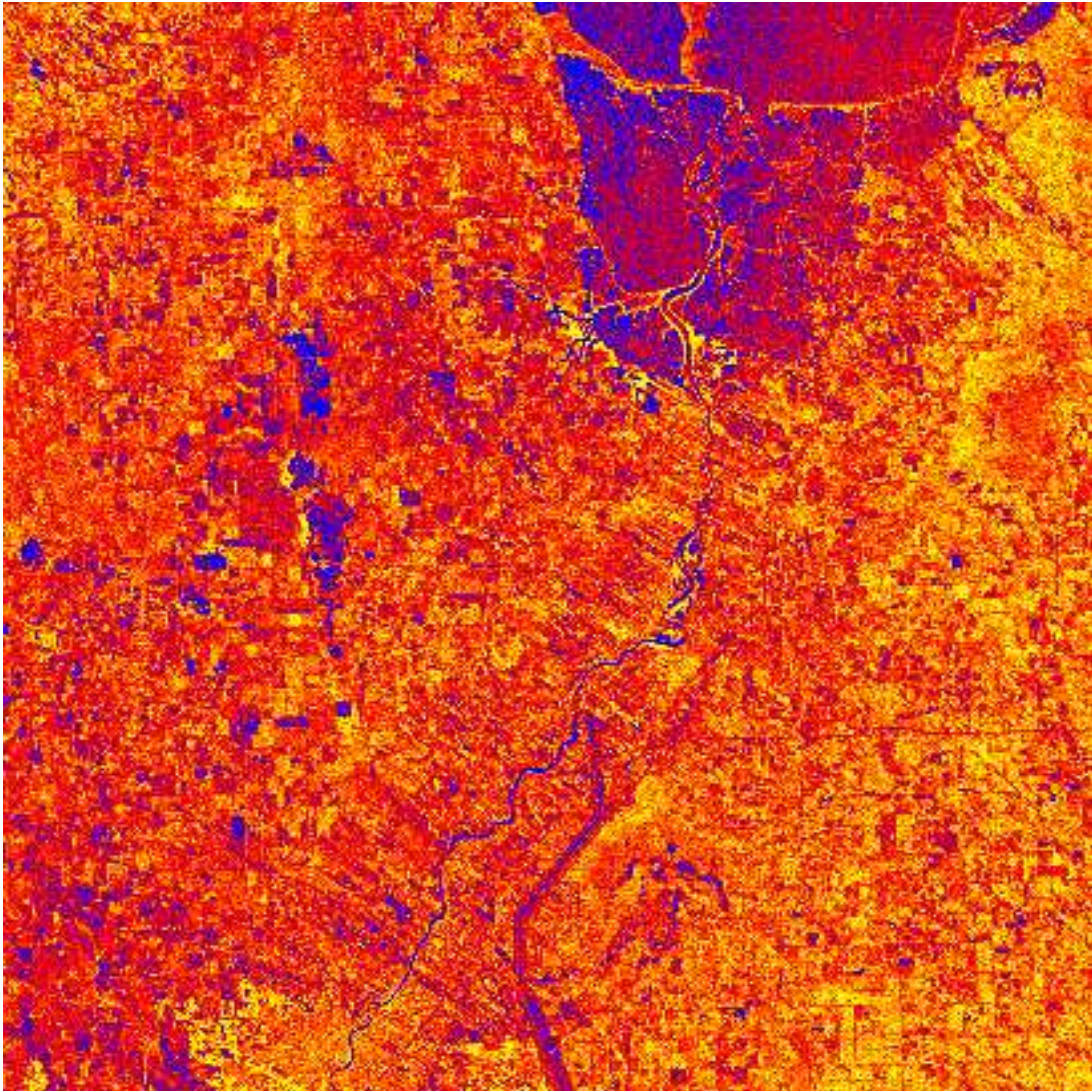


Figure 25: Red River flood in Manitoba captured on May 11, 1997 by Landsat

### *3.6.2 Flood Prediction Through Observation of Clouds*

Another use of remotely sensed data in flood management is in forecasting of floods based on the presence of rain-bearing clouds. Flood prediction based on monitoring the

clouds associated with heavy rain can be achieved using satellite imagery. Figures 26 (a), (b) and (c) illustrate METEOSAT (geostationary meteorological satellite) images in the visible, infrared and water vapor bands. After correcting them to account for varying illumination times and angles, seven categories of cloud classes can be identified. The analysis can also be supported by temperature and humidity profiles from radiosondes in the wider geographical area as well as by synoptic maps of the area.

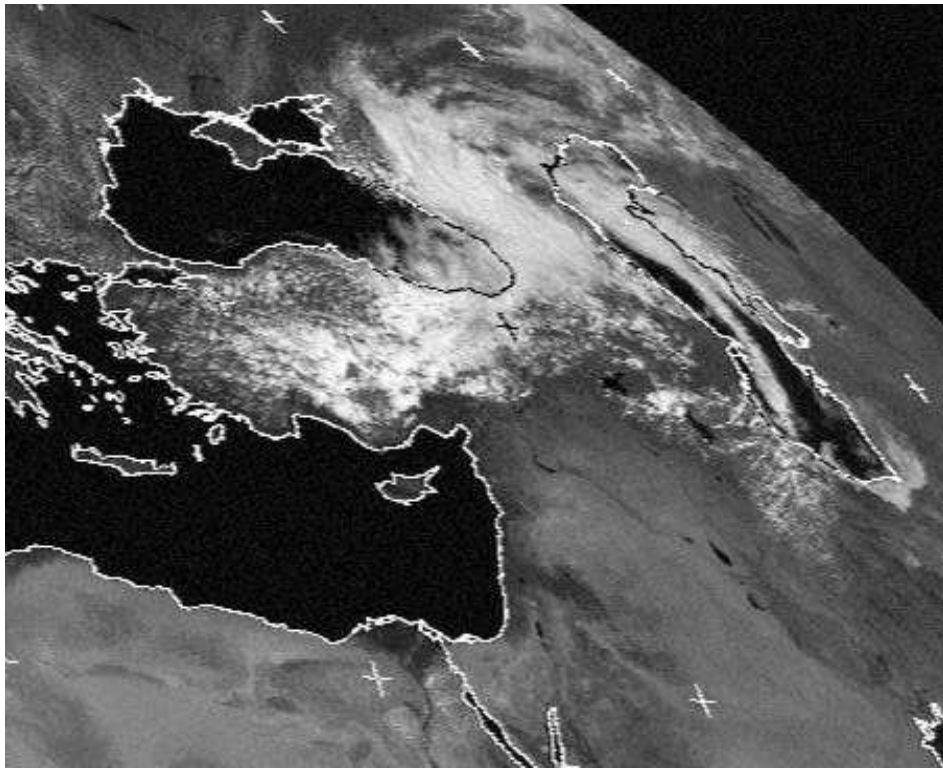


Figure 26 (a): METEOSAT image in visible band (source: <http://meteosat.e-technik.uni-ulm.de/meteosat/images/mono/>)

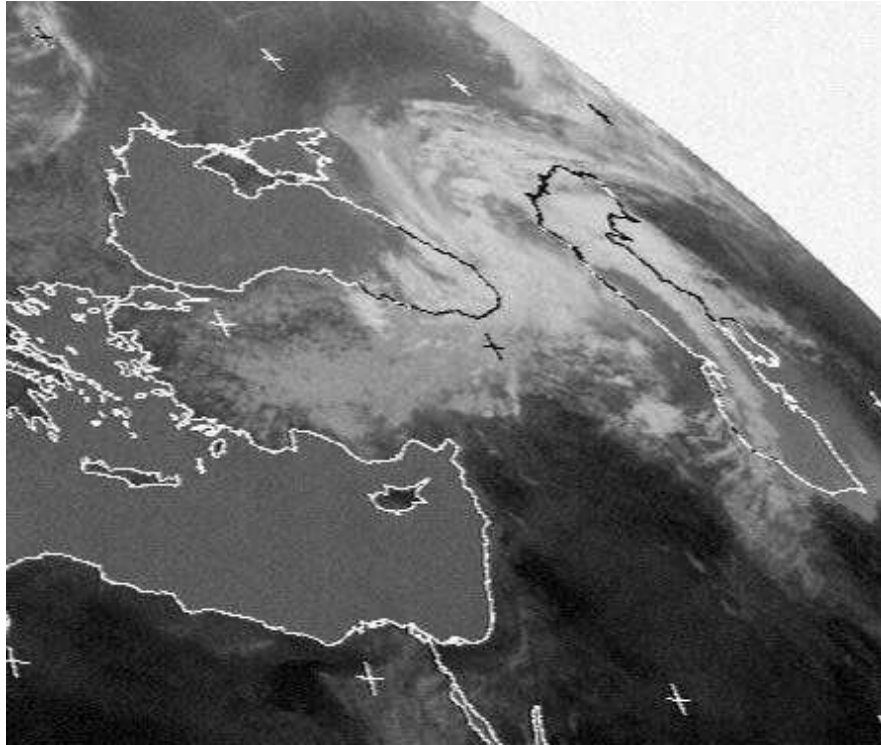


Figure 26 (b): METEOSAT image in infrared band (source: <http://meteosat.e-technik.uni-ulm.de/meteosat/images/mono/>)

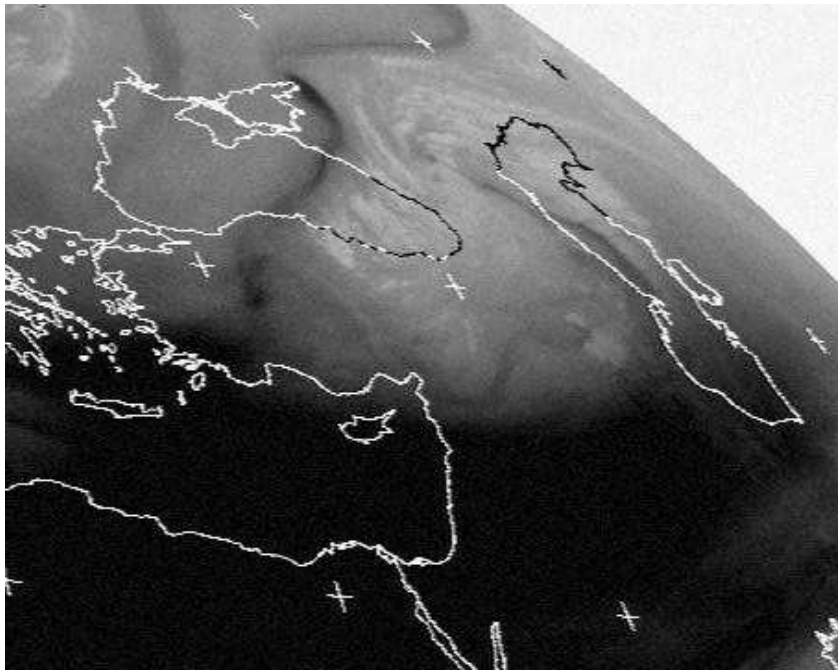


Figure 26 (c): METEOSAT image in water vapor band (source: <http://meteosat.e-technik.uni-ulm.de/meteosat/images/mono/>)

Feidas et al (2000), classified METEOSAT images from two flood incidents that occurred in Greece in October 1994 and January 1997 on the basis of the defined cloud categories and cloud cells associated with heavy rain. These clouds were clearly depicted on the classified images as thick opaque convective clouds.

At the UK Meteorological Office, pattern recognition techniques are being evaluated to see how information on cloud types, cloud systems and other meteorological parameters can be extracted from satellite imagery. One such technique is the neural network. It can be used for identifying the cloud, by identifying and training cloud patterns in the imagery. Once trained, the neural network is able to recognize the cloud types in other images. A neural network has been successfully trained to differentiate the types of airmasses, either dynamic or convective, needed for a flood forecasting (Pankiewicz, 1997). The airmass classification determines whether to use a precipitation forecast model based on extrapolation techniques, or an object-oriented convective precipitation forecast model based on a conceptual model of convective cells. Figure 27 is an illustration of cloud classification using neural network technique.

### **3.6.3 The Snow Factor**

About 50% of the annual precipitation in North America is stored in the snow reservoirs. The state of this snow pack during the melt period in spring is vital for the development of flooding in the catchment as the areal snow extent is directly related to the surge-type runoff potential. Though, the water-equivalent depth of a wet snow pack cannot be derived from remotely sensed data, the derivable snow cover fraction is an important

parameter to monitor for operational flood forecasting. The amount and rate of runoff induced by melt processes in the snow pack is definitely a function of the snow cover

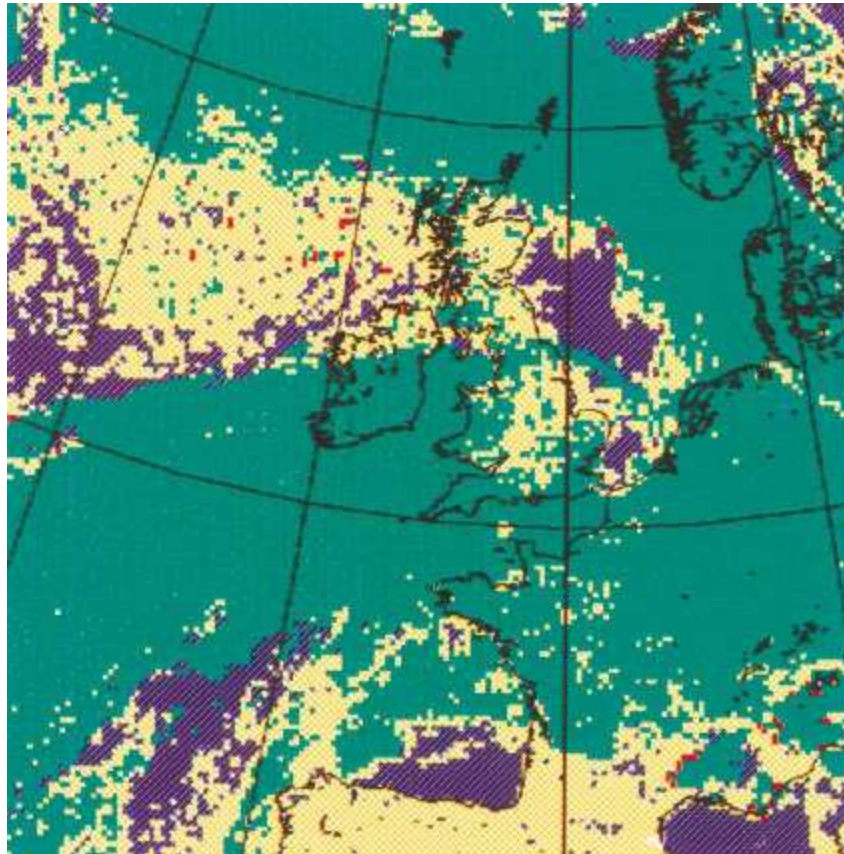


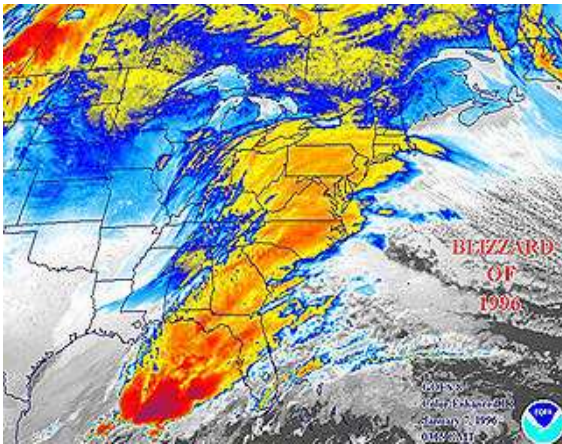
Figure 27: Cloud classification by a neural network. Purple - clear land and sea; green - dynamic cloud; yellow - shallow convective cloud and red – deep convective cloud (source: <http://www.eumetsat.de/en/>)

fraction for a given climatic condition. In the case of heavy rainfall combined with snow melt the flooding can be an extreme and rapid event. Optical, passive and active microwave sensors can acquire snow measurements from satellite. Snow-characteristics and hydrological-runoff models can be coupled, so that remotely sensed snow data can be used to adjust the model variables. In this way, remote sensing can enhance the



understanding of mountainous watershed behaviour and significantly improve the accuracy of streamflow forecasts (<http://www.geog.ubc.ca>). The main snow parameters affecting the runoff include snow covered areal extent, albedo, snow depth, snow water equivalent and snow wetness/onset of melt.

Major snow storms can cause heavy cover that leads to extensive flooding, if a rapid thaw occurs. GOES-8 coverage in Figure 28 (a) shows a massive storm that hit the northeastern U.S. on January 7, 1996. Image in Figure 28 (b), taken after storm passage and return of clear skies, shows the extent of snow cover. A combination of ice, followed by more than 50 cm of snow, and then a rapid thaw led to basement flooding in the houses located on the side of a hill, away from any floodplain.



(a)



(b)

Figures 28 (a) and (b): The GOES-8 images of the northeastern U.S. on January 7, 1996 (source: <http://www.fas.org/>)

Depending on snow cover properties, such as liquid water content, grain size, snow density and distribution of ice layers, backscattered radar pulses allow insight into the snowpack. Spatially distributed SAR data is, therefore, well suited to analyze snow cover dynamics. Sensor characteristics offer the possibility to discriminate between the dry snow, the percolation and the wet snow zones of a glacier (Rau & Saurer, 1998). Automatic generation of snow cover maps might help as it can be used as input for operational runoff modeling and forecasting. Nagler et al (1998) and Maxfield (1999) used SAR images, single channel and multi-temporal, to study the change detection of the backscattering coefficient between repeat pass images of snow covered surfaces and reference images so as to generate snow cover maps. SAR data has proven useful in detecting open water surfaces, near-surface moisture, soil moisture changes and the extent of wet snow packs, therefore, it is feasible to distinguish between wet snow and dry snow and between wet ground and dry ground where no snow cover is present. This way it would also be possible to create a series of snow cover maps over the period of the snowmelt season to roughly quantify rate of snowmelt in the catchment (Hillard et al, 1999).

Some studies (late 80s) based on ground-based scatterometer have shown the possibility of active microwave remote sensing to measure snow water equivalent (SWE) for “simple” snowpack, especially dry snow. There has not been enough data to understand the relationship between microwave backscattering coefficient (BSC) and physical properties of wet snow. Fukami et al (1999) have shown in their study that the relationship between BSC and SWE shows negative correlation for the case  $SWE < 200 - 300$  mm, but positive for  $SWE > 200 - 300$  mm. Dedieu et al (1997) analyzed the

signature of snow-covered high alpine terrain for different snow surface and volume conditions and inferred that high incidence angles of SAR data are necessary in mountainous areas for corrections of slope effects, and that the ascending or descending modes lead to different backscattering of snow-covered terrain. SAR image can be useful to record the river-ice break up - as the ice (and snow covering it) melts, backscatter decreases (Murphy et al, 1998). Murphy showed that from 25 days to 1-½ days before breakup the ice texture changed from mottled to a distinct patchy pattern with circular, transverse and longitudinal bright linear features. One and half days before breakup cracks, rubble ice and pressure ridges increased and RADARSAT SAR images have good potential for aiding in the prediction of river ice breakup because of changes in the ice backscatter as breakup approaches.

NOAA-AVHRR sensors, as pointed out by Schjødt-Osmo and Engeset (1999), are good to derive information on the changing distribution of snow during periods of accumulation and, in particular, ablation. Through classification, water bodies, clouds, bare ground, and a set of snow cover classes, based on the fractional percentage of snow cover within each pixel, could be separated. Routinely, images from the NOAA and the GOES satellites can be used to determine the extent of snow cover. We can separate snow from clouds by differences in spectral absorption in longer wavelength bands. Both are highly reflective in the visible and photographic IR. The TM band 5 also can distinguish snow/clouds. A color composite made from three NOAA-12 AVHRR bands (1,3,4 = RGB) is illustrated in Figure 29 showing snow in April 1995 in the northwestern U.S. as red.

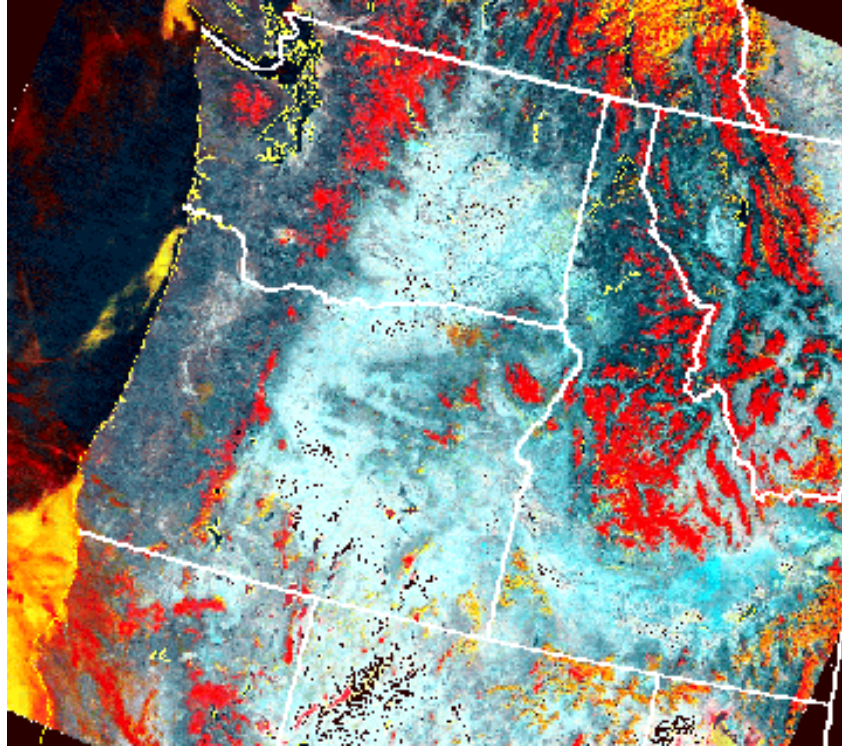


Figure 29: NOAA-12 AVHRR image captured in 1995 showing snow in red (source: <http://www.fas.org/irp/imint/docs/rst/Front/>)

#### **4. GEOGRAPHIC INFORMATION SYSTEM**

Population increase and migration into areas under threat of natural hazards is a global concern. Earthquakes, tsunamis, volcanoes, cyclonic storms and floods endanger increasing populations and their sustaining agriculture.

Geographic Information System (GIS) is a vital tool for making use of remotely sensed data for disaster mitigation. High resolution visible and SAR images are good for extracting topography and preparing land use maps of any area. Digital Elevation Model (DEM) and land use map are important inputs to flood simulation models.

Lanza and Conti (1994) have discussed the potential of joining remotely sensed information and hydrologically oriented GIS structures to assist in flood forecasting. The remaining issues include different resolution scales, which are associated with data observed by the available sensors and their hydrological interpretation. The joint use of the various sensors is proposed in order to address the problem of quantitative precipitation forecasting at the small scale. The GIS data handling capability plays a major role in supporting the effectiveness of automated procedures eventually developed for flood hazard control in highly urbanized areas.

Studies addressing the role of remotely sensed geographic information in mitigating "instantaneous" disasters, such as floods, have resulted in the following list of potential applications (Verstappen, 1995):

- Establishment of susceptibility of the land and vulnerability of the society;
- Mapping potential hazard areas for use in physical planning (hazard zoning maps);
- Monitoring potentially hazardous situations and processes, providing advanced warning; and
- Improvement in management of emergency situations following a disaster.

Remotely sensed data, hydrologic models and GIS techniques can be combined to simulate potential flooding. According to a study on Swan Creek in Ohio, U.S. at Bowling Green State University, U.S., a combined method of linking a GIS with flood modeling software (e.g., HEC-RAS) is a cost and time efficient method for planning

damage mitigation measures. In this study different time period aerial photos (Figure 31) were used to get a land use map with changes detected as shown in Figure 32. Using the Rational Equation (Equation 1), a rain event can be combined with the land-use to approximate the water that will flow into the channel.

$$\text{Discharge (Q)} = C * I * A \quad (1)$$

Where C is a coefficient; I is inflow ( $\text{m}^3/\text{sec}$ ) and A is area ( $\text{m}^2$ )

From the information on the discharge and assistance of the hydrologic model a flood extent can be presented as shown in Figure 31. Map as shown in Figure 33 can help in the determination of water depth and flood damage. For emergency management purposes flood extent overlay on remotely sensed scene of the area, like in Figure 34, can be of great assistance. This approach can help the regional planning authority in planning for and mitigating the effects of urbanization in any fast developing region.

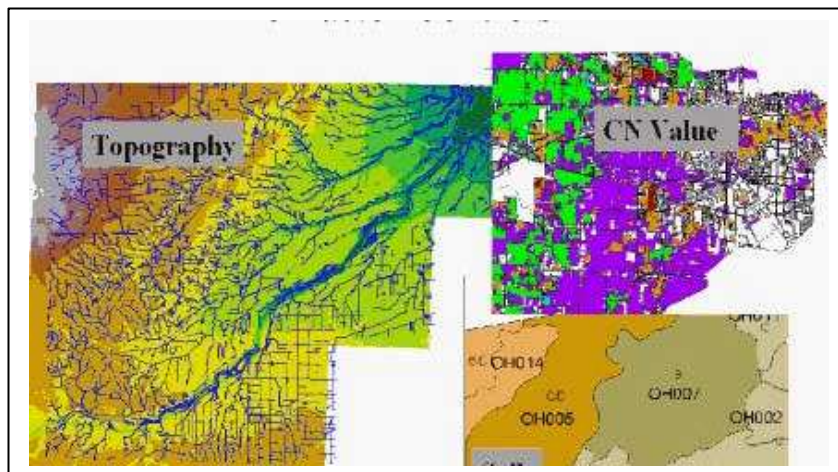


Figure 30: C factor map obtained for Swan Creek, Ohio, USA (source: <http://nsl.bgsu.edu/swancreekrap/>)

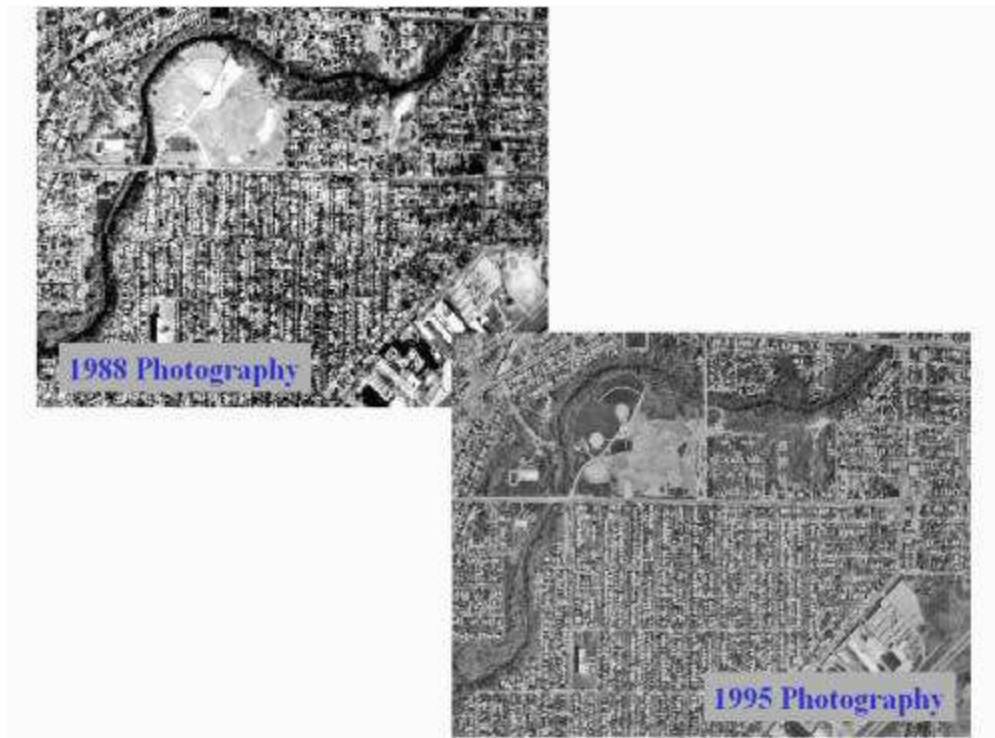


Figure 31: Aerial photos of two different years to assess the urbanization in the catchment (source: <http://nsl.bgsu.edu/swancreekrp/>)



Figure 32: Land use thematic layer (source: <http://nsl.bgsu.edu/swancreekrp/>)



Figure 33: Flood extent and depth (source: <http://nsl.bgsu.edu/swancreekrap/>)

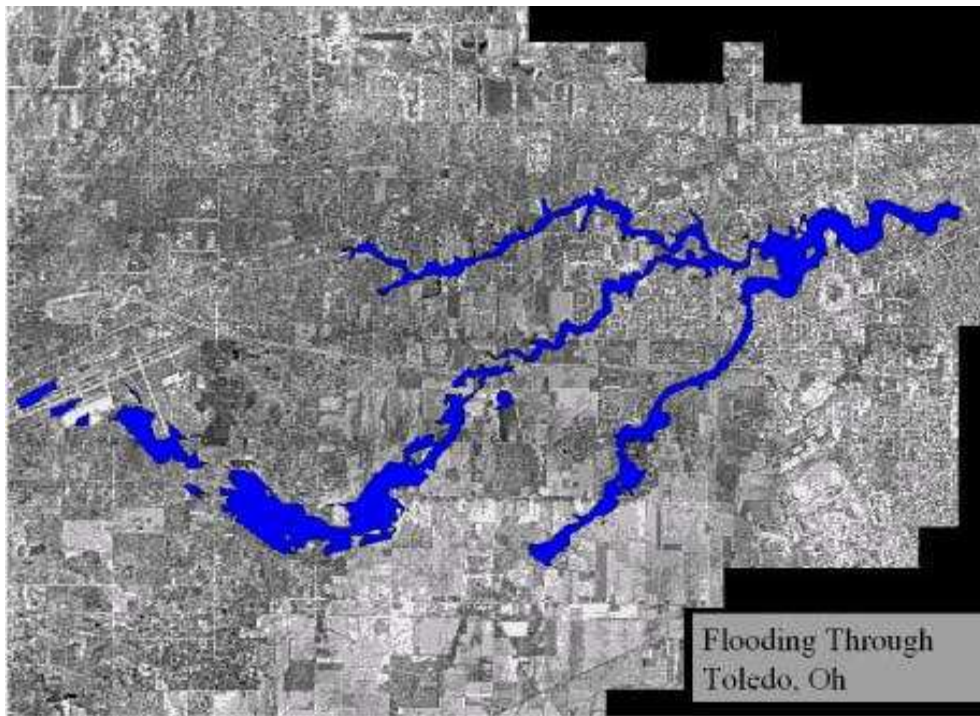


Figure 34: Overlay of flooding scenario on remotely sensed scene of the area (source: <http://nsl.bgsu.edu/swancreekrap/>)



## 5. WEB TECHNOLOGY

The fast developing web-technology has prompted the scientists, experts and educators to start developing web-based decision support tools that allow planners and other government decision makers to utilize a high-resolution DEM and floodplain related GIS data layers in making floodplain management decisions. Weather forecasts are based on satellite-captured images, which can be accessed through the Internet. Cyclones, tsunamis and hurricanes can be seen coming through the satellite images. Movement of high/low pressure winds can be monitored at 5-minute interval to help scientists simulate the future scenario. Forecasting and warning regarding natural disasters can easily be made available on the Internet. When any disaster seems to be occurring at one geographic location, Internet tools help the other locations in the world, where people and property might get affected by the same disaster in due course of time, take precautionary actions. Knowledge of flow rate and speed of an occurring flood helps predict its impact in other downstream areas. Similarly, cyclones, forest fires and volcano lava flow can be observed and monitored in real time using Internet tools. Thus the Internet technology has become a vital tool in disaster management through sharing of information.

Simonovic and Huang (1999) coined the concept of Virtual Data Base (VDB) for the management of floods making use of the Internet technology. The idea of VDB was conceived after the 1997 Red River floods, which prompted several other flood management and mitigation studies ([www.rrbdin1.org](http://www.rrbdin1.org)). Red River Basin Decision Support System (REDES), introduced by Simonovic (1999) was developed to enhance preparedness planning, response, and recovery with emphasis on flood prediction and

monitoring, emergency response, and public involvement. According to the International Red River Task Force (<http://www.ijc.org>), use of passive and active microwave satellite images visible and infrared images are recommended for flood management and damage assessment. Sugumaran et al (2000) have developed a tool using data for a small subdivision in St. Charles County in Missouri using digitally scanned National Aerial Photograph Program (NAPP) photos in conjunction with highly accurate ground control from a rapid-static Global Positioning System (GPS) survey. The design and Web-technology part was done using ArcView and Map Server GIS software, Java, JavaScript, HTML and Avenue programming. This Web-based interface would allow users to interactively display and query different floodplain-related GIS layers so as to know whether a parcel is within or outside the 100-year floodplain and determine the elevation of a particular point as well.

Animations of daily snow water equivalent for the U.S. are made available at <http://www.nohrsc.nws.gov/index.html> showing snow pack dynamics throughout the winter/spring season. An experimental modeling system being developed at the NOHRSC (National Operational Hydrologic Remote Sensing Center) to provide hourly snow hydrology information throughout the U.S. at 1-km spatial resolution is shown in Figure 35.

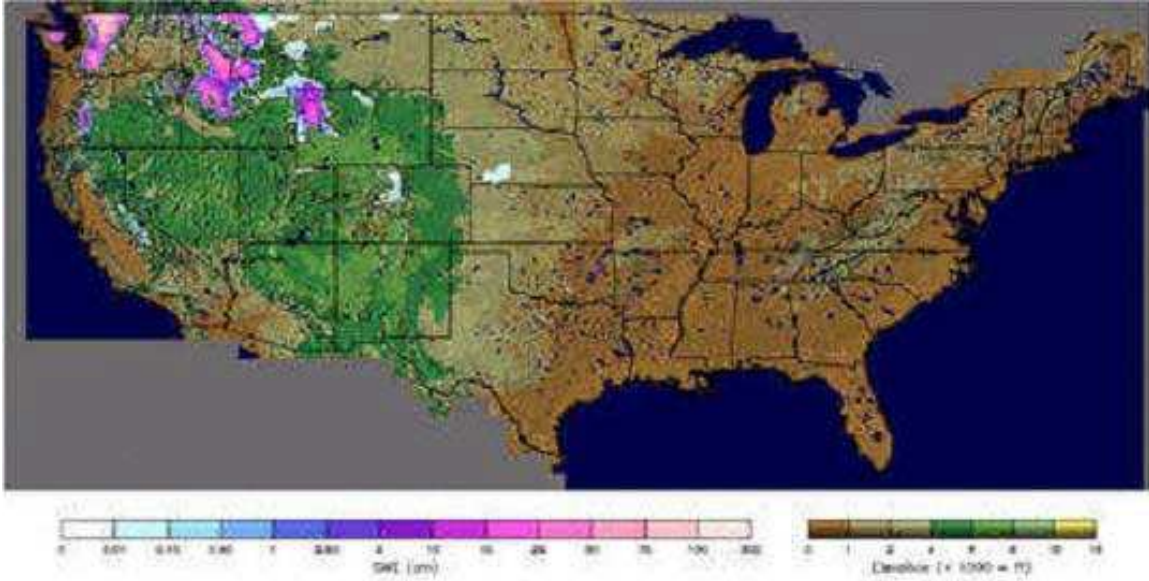


Figure 35: Snow water equivalent image (source: <http://www.nohrsc.nws.gov/index.html>)

## 6. CASE STUDY

Among various natural phenomena we get rainfall, snow and four seasons that keep varying the temperatures, soil moisture and humidity. In case of rain, rainwater saturates the soil before forming any overland flow. In case of snow, when the temperature rises, accumulated snow starts building up an overland flow that reaches the drainage channels finally. Does this quantity of overland flow and river flows remain the same when the land use changes dramatically in a particular way? To explore the possibility of finding a relationship between the urbanization and river flows remote sensing and Geographic Information Systems (GIS) techniques can be very useful.

Very powerful computers and smart software that are available today make it possible to carry out complicated and tedious computations necessary to process huge amount of data. Internet facility has amazing power of database sharing and real time processing of

data, which is vital in emergency management. Post-disaster data acquisition helps in the disaster recovery; damage claim process; fast compensation etc. Analysis of remote sensing data can help the mitigation process through better prediction; detection of disaster prone areas; location of protection measures and identification of resources. Through a case study the use of remote sensing in developing conservation policies has been demonstrated in this section.

Upper Thames River (UTR) watershed (Figure 36), where the city of London is experiencing net migration trends similar to those for Metropolitan Toronto, has been chosen for this case study. This case study illustrates the process of establishing a relationship between impervious area and river flows using remote sensing techniques and through analyzing the hydrologic and meteorological data. Findings from this case study can be used to form policies on land use planning and balanced urbanization by the city development, planning and conservation authorities. Once the affect of urbanization on river flows is quantified, the future trend would become possible to predict so that measures to cope with increasing demand for residential/commercial areas can be met without risking the increased intensity and extent of storm water in rainy periods.

The normally placid Thames was periodically subject to severe flooding which disrupted the new communities built in the river's extensive floodplains. The first written account of flooding after European settlement on the Thames River dates from 1791 and floods of various levels were recorded regularly after that. However, because of the long time interval between severe floods, residents tended to forget the potential for flooding and

built more in the floodplain than was wise. Other activities, such as clearing forests and draining wetlands, also increased the severity of floods.

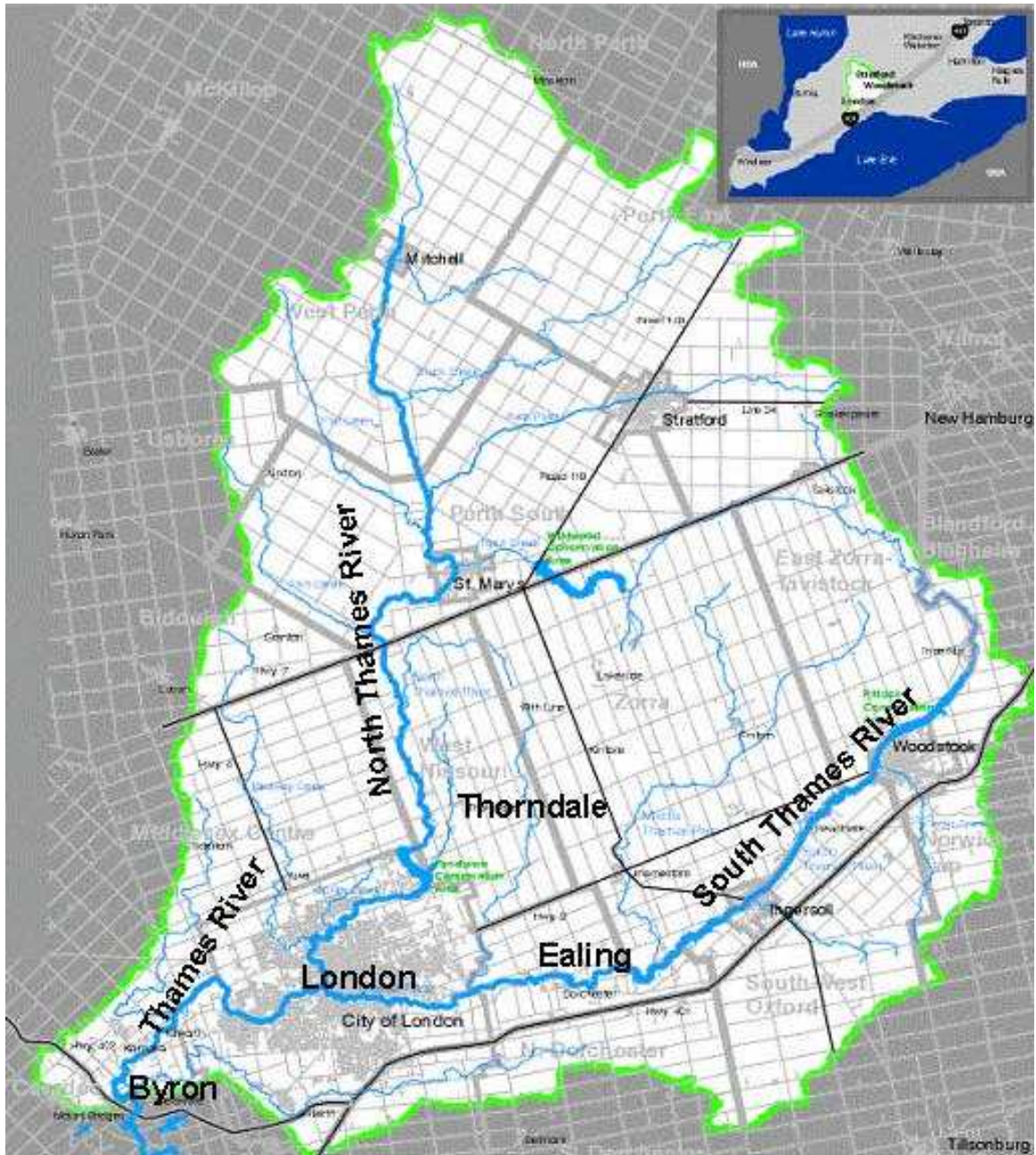


Figure 36: Upper Thames River Watershed in southern Ontario, Canada

Upper Thames River Conservation Authority (UTRCA) in southern Ontario takes up the task of flood control, preservation of agricultural lands, improved forestry management practices, water quality upgrading and other considerations which are important for ecosystem upkeep (UTRCA, 1994). Over last three decades (1971 to 2001) the population of the city of London has gone up by approximately 43%, which is expected to go up by a total of 67% by the year 2026 (UTRCA, undated). This case study will provide a methodology to be followed by conservation authorities making their task easier and their estimates more accurate.

## **6.1 Methodology**

### *6.1.1 Land use Classification of Satellite Imagery*

Reflections measured by satellite sensors depend on the local characteristics of the earth's surface, which should be found out in order to extract information from the image data. Theoretically, a single spectral band of a remote sensing image should be enough to carry out classification, however, multi-spectral band classification gives much better results. Using image processing software satellite images of different time period for the same area were processed and analyzed. To do so, first of all, *signatures*, which are statistical characterizations of each information (land use) class, were created. There are three main classification techniques, namely, the Parallelepiped procedure (included only for pedagogic reasons), Minimum Distance procedure (should be used when there are concerns about the quality of signatures) and Maximum Likelihood method (should be

used when signatures are known to be strong). A brief description of all the three methods is as follows;

*Minimum distance:* The minimum distance rule calculates the spectral distance between the measurement vector for the candidate pixel and the mean vector for each signature. The candidate pixel is assigned to the class whose mean is the closest. The equation for classifying by spectral distance is based on the equation for Euclidean distance (ERDAS, 1991).

$$SD_{.xyc} = \sqrt{\sum_{i=1}^n (\mu_{ci} - X_{xyi})^2} \quad (2)$$

Where  $n$  = number of bands (dimensions);  $i$  = a particular band;  $c$  = a particular class;  $X_{xyi}$  = data file value of pixel  $x,y$  in band  $i$ ;  $\mu_{ci}$  = mean of data file values in band  $i$  for the sample for class  $c$  and  $SD_{.xyc}$  = spectral distance from pixel  $x,y$  to the mean of class  $c$ .

When spectral distance is computed for all possible values of  $c$  (all possible classes), the class of the candidate pixel is assigned to the class for which  $SD$  is the lowest.

*Parallelepiped:* In parallelepiped decision rule, the data file values of the candidate pixel are compared to upper and lower limits. These limits can be either: (i) the minimum and maximum data file values of each band in the signature, (ii) the mean of each band, plus and minus a number of standard deviations, or (iii) any limits that you specify, based on your knowledge of the data and signatures. In the cases where a pixel may fall into the overlap region of two or more parallelepipeds, it is assigned to the first class tested (ERDAS, 1991).

*Maximum Likelihood Method:* The Maximum Likelihood method is based on Bayesian probability theory. It uses the mean and variance/covariance of signatures to estimate the posterior probability that a pixel belongs to each class. Maximum Likelihood procedure accounts for intercorrelation between bands, therefore, the information about the covariance between bands as well as their inherent variance is included thus producing elliptical zone of characterization of the signature. In fact, it calculates the posterior probability of belonging to each class, where the probability is highest at the mean position of the class and falls off in an elliptical pattern away from the mean, as shown in Figure 37 (Eastman, 2001). Mathematically, the procedure can be explained as (Gorte, 2000):

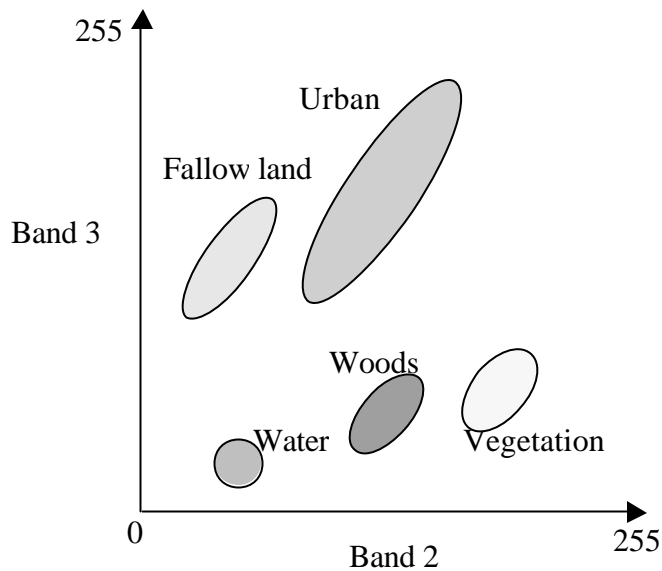


Figure 37: Maximum Likelihood procedure



Let there be a set of  $N$  classes  $C_1, \dots, C_N$  and  $C_i$  is assigned as ‘most likely’ class to any feature vector  $x$  in an image. The most likely class label  $C_i$  for a given feature vector  $x$  is the one with the highest posterior probability  $P(C_i/x)$ . Each  $P(C_i/x)$ ,  $i \in [1..N]$ , is calculated, and the class  $C_i$  with the highest value is selected. The calculation of  $P(C_i/x)$  is usually based on Bayes formula:

$$P(x/C_i) = \frac{P(x | C_i)P(C_i)}{P(x)} \quad (3)$$

Where  $P(x/C_i)$  - class probability density;  $P(C_i)$  - prior probability and  $P(x)$  - feature probability density (class-independent).

The disadvantages of *minimum distance* method are that it does not consider class variability. For example, if an urban land cover class is made up of pixels with a high variance, which may tend to be farther from the mean of the signature, *minimum distance* classification method might improperly classify outlying urban pixels. Inversely, a class with less variance, like water, may tend to get overclassified because the pixels that belong to the class are usually spectrally closer to their mean than those of other classes (ERDAS, 1991). *Parallelepiped* method’s problem is that the pixels falling in overlapping parallelepipeds or that fall outside any parallelepipeds are not taken care of properly. Also, since parallelepipeds have corners, pixels falling in them may be classified which are actually quite far, spectrally, from the mean of the signature. Advantage of *maximum likelihood* method is that it takes the variability of classes into account by using the covariance matrix (ERDAS, 1991). Therefore, Maximum

Likelihood supervised classification technique was chosen to apply to the images used in this case study to classify them in seven land use category, such as, woods, row crops and legume grasses, small grain or grasses, fallow land, urban/city, homestead and open water bodies. These land use classes coincide with the Upper Thames River Conservation Authority (UTRCA) land use classes according to UTRCA's 1983 land use map (UTRCA publication, 1983).

### *6.1.2 Hydrologic data analysis*

City of London in UTR watershed is the main concern in this case study. One hydrologic data measurement station, which would represent the inlet and another hydrologic data measurement station, which would represent the outlet of the study area, were chosen for daily river flows time series acquisition. Similarly, another representative meteorological measurements station was chosen for daily total precipitation (rainfall + snow) time series. All the three time series (two river flows series and one total precipitation time series) were plotted together to get the peak flows pattern as well as the time to peak at inlet and outlet points of the study area. Also, the difference in peak flows at inlet and outlet stations would give an idea of the affect of the urbanization because the inlet station is at the upstream of the major city and outlet station is located just outside the city at the downstream.

Land use/cover classification results would illustrate the changes in land use over three decades. In particular increased urban area would imply increased impervious region.

Integrating the analyzed hydrologic and meteorological data and classification findings would indicate the effect of urbanization on river channel flows.

### 6.1.3 Description of study area

Upper Thames River watershed, which is the second largest in southwestern Ontario, is in Canada. Total area of the watershed is 3482 km<sup>2</sup>, which falls within central meridian of 81W, Zone 17 and length of drainage basin is 200 km covering the north and south branches of the Thames River (UTRCA, 2001). The watershed is mainly rural except for the larger urban centers of London, Stratford and Woodstock and has a population of over 400,000. The industrial sector within the watershed is based around automotive assembly and supply, aggregate extraction for the construction industry, and agricultural based industries. Agriculture is the main component of the landscape with approximately 3,600 farms, including over 2,000 livestock operations. The Thames River is much more responsive to climate changes than the larger Great Lakes area. Precipitation, or lack of it, can quickly cause conditions to change in the Thames River watershed. For example, stream flows were greatly reduced in the Thames River watershed in 1998 and 1999 causing many watercourses to dry up completely. The rate of runoff into the two branches of Thames River is too high and floods may occur at any time of the year, but it is the floods which occur during the spring break-up that are most frequent and most severe. The impervious clay soils, the high gradient of the riverbed, and the steep lateral slopes of the tributaries increase the rate of runoff (UTRCA publication, 1955). There are 20 sub-watersheds, 26 hydrologic observation stations, managed by Environment

Canada, in the Upper Thames River watershed, out of which about 10 observation stations are on or near the Thames River. Hydrologic measurements at Thorndale (upstream inlet point) and Byron (downstream outlet point) have been used in this study. The north branch of Thames River is regulated by Fanshaw dam (since 1952), which is located north of city of London and downstream of Thorndale. Thorndale hydrologic measurement station records unregulated inflow into Fanshaw reservoir. Therefore, river flows at Thorndale are being used for analyzing the observed river flow time series. On the south branch of Thames River Pittock reservoir (since 1965) does not affect the flows at Ealing (Figure 34) observation station because it is quite far upstream from London. Byron measurement station, which is located south of London where the flow is measured and used in this study, can be considered the outlet point for the entire watershed. Though, total precipitation time series are available at London, Stratford and Woodstock meteorological stations managed by Environment Canada, only the time series of total precipitation at London has been used for the analysis purpose in this study because the affect of urbanization in London is the main focus here.

## **6.2 Data Analysis and Results**

### *6.2.1 Remote Sensing Data Analysis*

Three imagery of LANDSAT satellites covering the Upper Thames River watershed were acquired over the time period of 1974 to 2000. Though LANDSAT-1 was launched in 1972, no clear (cloud-free) image could be found for the study area before 1974. Within the constraints, three images that are included in this study are LANDSAT-1 MSS (Multi

Spectral Scanner) of July 7, 1974, LANDSAT-5 TM of July 23, 1990, and LANDSAT-7 ETM<sup>+</sup> (Enhanced Thematic Mapper) of October 30, 2000. To be able to see the details in satellite imagery more clearly, while MSS image of LANDSAT-1 was converted into colour composite of bands 2 (0.6 – 0.7 $\mu$ m), 3 (0.7 – 0.8 $\mu$ m) and 4 (0.8 – 1.1 $\mu$ m), LANDSAT-5 image was converted into colour composite of bands 3 (0.63 – 0.69 $\mu$ m), band 4 (0.76 – 0.9 $\mu$ m) and band 5 (1.55 – 1.75 $\mu$ m) and ETM image of LANDSAT-7 was converted into a colour composite of bands 3 (0.63 – 0.69 $\mu$ m), 4 (0.76 – 0.9 $\mu$ m) and 5 (1.55 – 1.75 $\mu$ m). Spectral resolution of LANDSAT-1 MSS image is 80 m and that of LANDSAT-5 TM and 7 ETM image is 30 m. Therefore, the different land use classes are more clearly visible in LANDSAT-5 and 7 images compared to LANDSAT-1 image.

Results of *Maximum Likelihood* supervised classification carried out on LANDSAT-1, 5 and 7 images are given in Figures 38, 39 and 40. Details of land use classes and their corresponding areas are given in Table 2.

Table 2: Land Use Classification Results for LANDSAT-1, 5 and 7 Images

| <b>Land Use Classes</b>                   | <b>LANDSAT-1<br/>MSS<br/>Jul 7, 1974<br/>(percent)</b> | <b>LANDSAT-5<br/>TM<br/>Jul 23, 1990<br/>(percent)</b> | <b>LANDSAT-7<br/>ETM<br/>Oct 30, 2000<br/>(percent)</b> |
|---|--|--|---|
| <b>Woods</b>                              | 24.01  | 11.98  | 13.06   |
| <b>Row Crops &amp; Legume<br/>Grasses</b> | 22.78  | 29.18  | 13.20   |
| <b>Small Grains or Grass</b>              | 31.56  | 34.91  | 16.84   |
| <b>Fallow Land</b>                        | 4.79   | 2.34   | 30.06   |
| <b>Urban</b>                              | 10.07  | 16.72  | 22.25   |
| <b>Homestead</b>                          | 3.14   | 2.05   | 1.86  |
| <b>Water</b>                              | 3.65   | 2.82   | 2.73  |

As it is clear from the values given in the table that tremendous urban development has taken place over three decades amounting to 22.25% urban region in 2000 as compared to only 10.07% in 1974. Areas covered by woods came down to 11.98% in 1990 but rose again to 13.06% in 2000. There is also a very significant difference in the percentage of row crops and legume grasses and small grains or grasses. Fallow land percentage is varying due to the different time of image acquisition of LANDSAT 5 and 7. Also, homestead percentage drops from 3.14% in 1974 to 1.86% in 2000. The difference in water availability over three decades can be noticed as well.

### *6.2.2 Hydrologic Data Analysis*

Observed total precipitation (rainfall and snowfall) and river discharge measurements were plotted to illustrate the actual changing trend of peak flows during the years 1970 to 1997. Hydrologic observation station, Thorndale is located upstream of London and hydrologic observation station, Byron is located south of London at the outlet of UTR watershed (Figure 36). The differences in peak flows between Thorndale and Byron, when plotted (Figure 41), show a mixed pattern over the years.

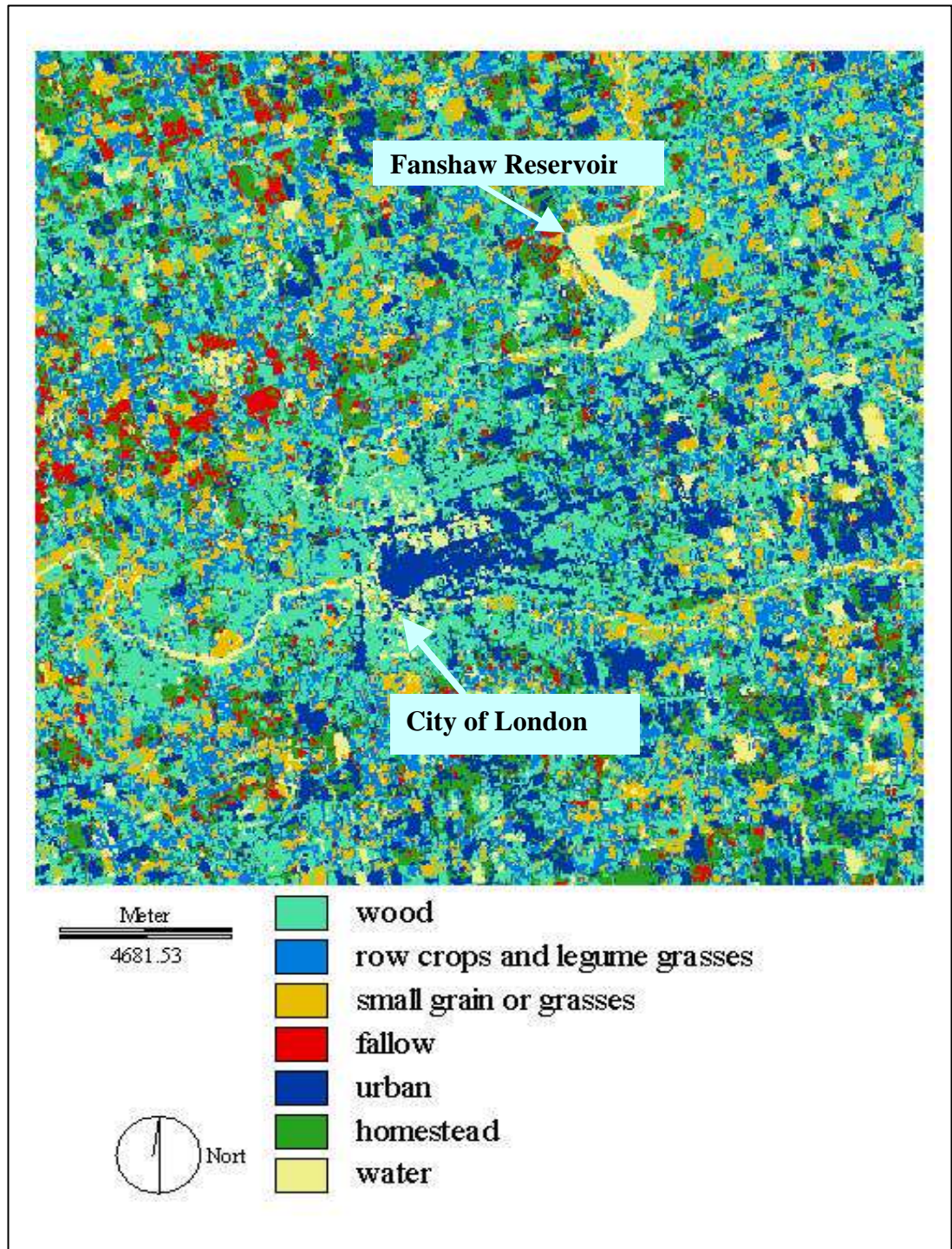
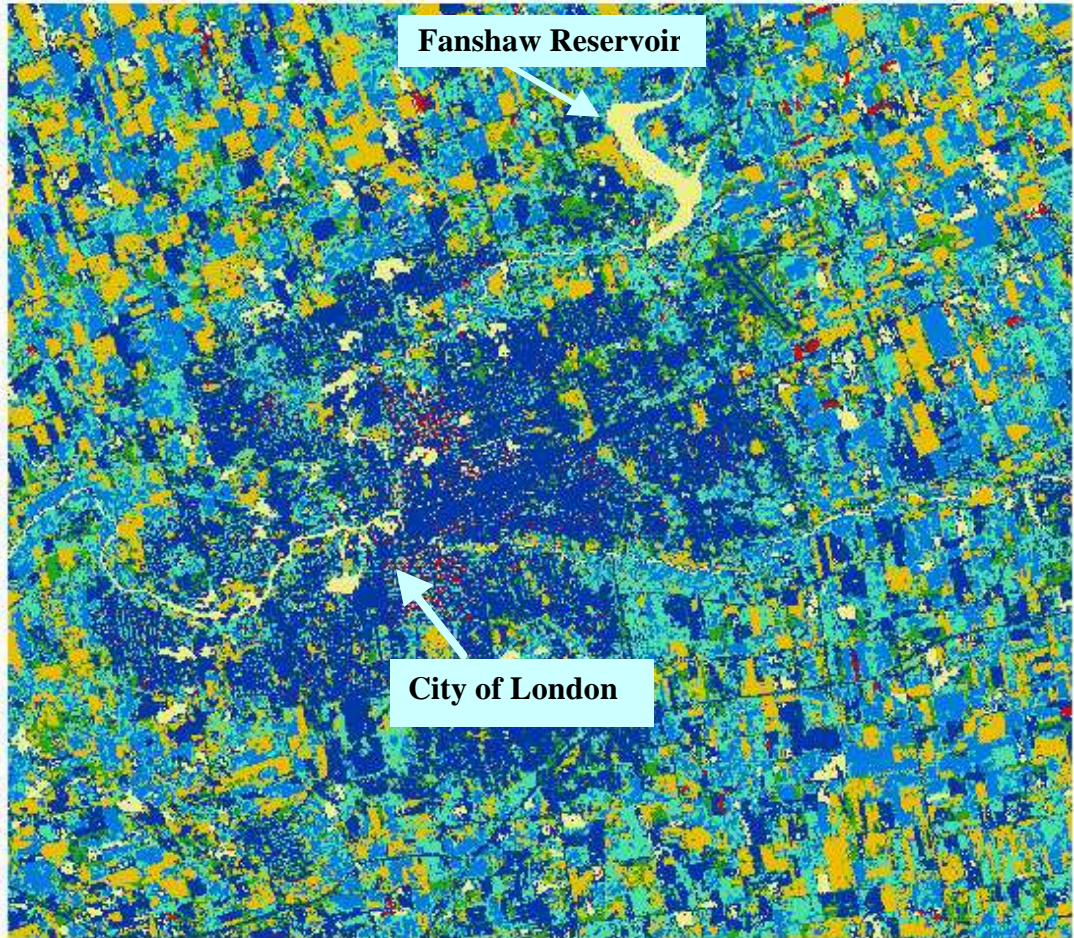
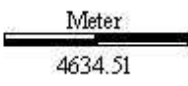








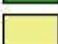
Figure 38: LANDSAT 1 Image classified for land use



Fanshaw Reservoir

City of London



-  wood
-  row crops and legume grasses
-  small grain or grass
-  fallow
-  urban
-  homestead
-  water

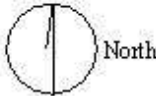




Figure 39: LANDSAT 5 Image classified for land use

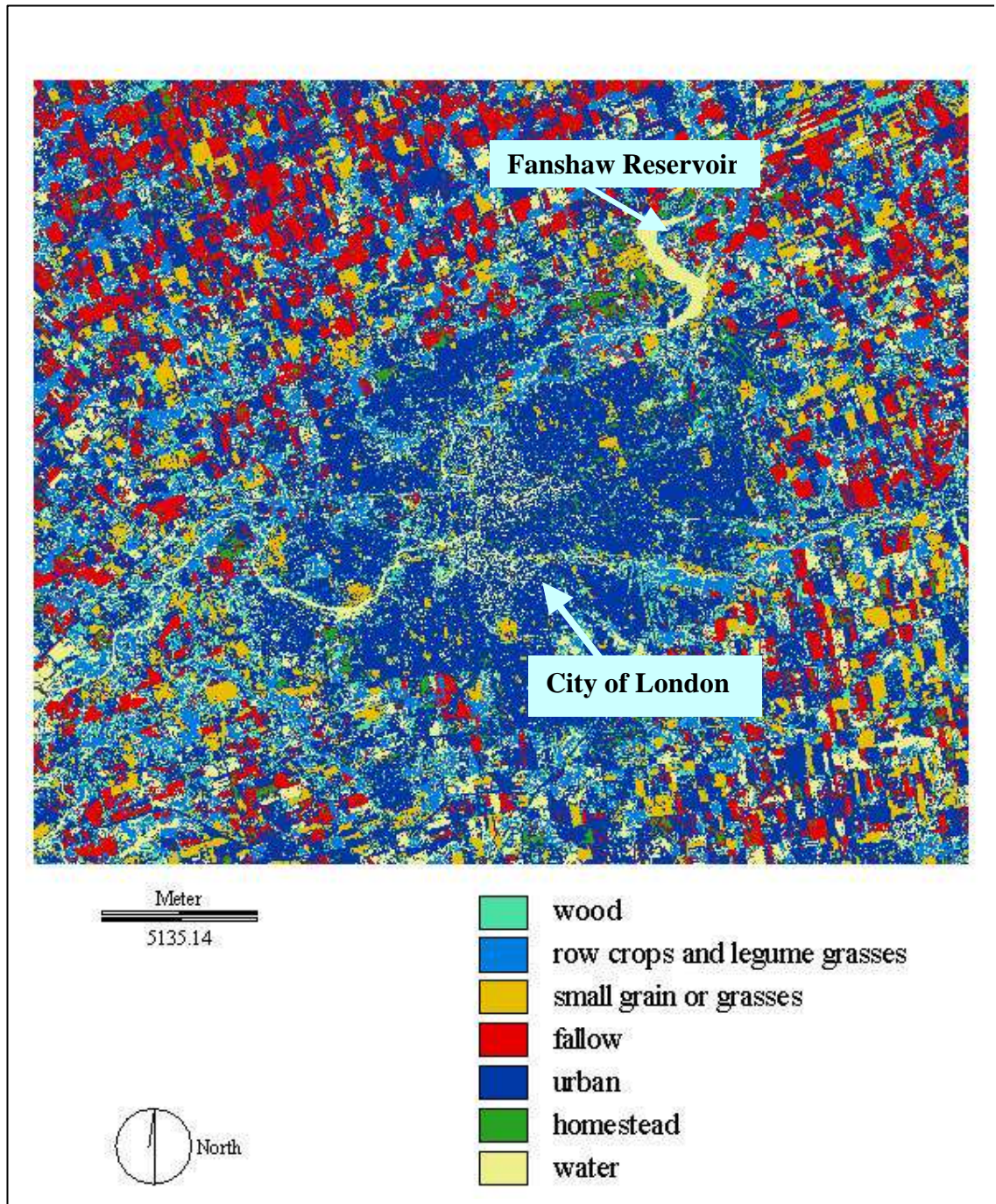


Figure 40: LANDSAT 7 Image classified for land use

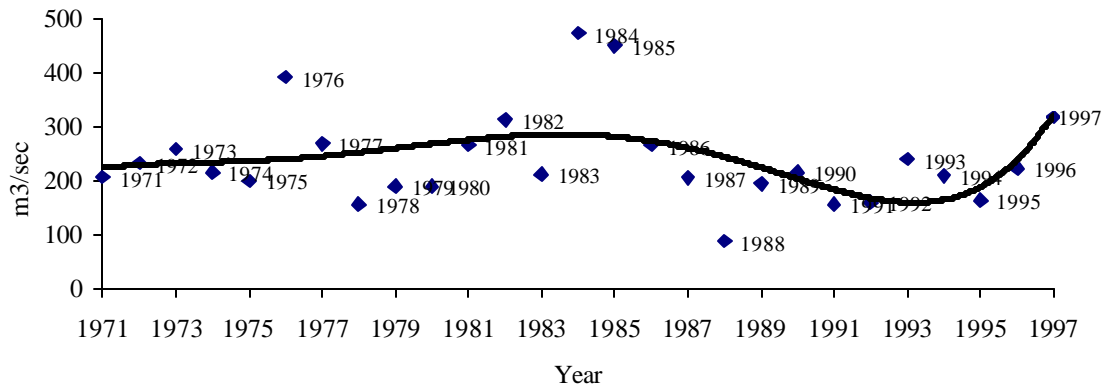


Figure 41: Plot of differences in observed peak flows at Thorndale and Byron

Figure 42 - 50 are plots of observed flows at Thorndale and Byron and total precipitation at London plotted together to have an understanding of the flow response to total precipitation occurred during each particular year. 1970 hydrographs at Byron and Thorndale, in Figure 42, plotted against total precipitation indicate a peak flow of about 300 m<sup>3</sup>/sec for a total precipitation of about 400 mm. As demonstrated in Figure 43, in 1976 a total precipitation of the order of 300 mm to 500 mm brought high flows of 660 m<sup>3</sup>/sec at Byron thus resulting in high peak flow difference between Thorndale and Byron, which means that the high peak flow difference was due to high total precipitation that year. In 1983 (Figure 44) the peak flow difference between Byron and Thorndale is due to the low total precipitation. However, the precipitation increased from the middle towards the end of the year bringing the flows at the beginning of 1984 to another high (Figure 45). Similar pattern of precipitation can be seen in 1985 (Figure 46) flows, which is the result of over 400mm of continuous precipitation between the 50<sup>th</sup> and 100<sup>th</sup> day of the year. The peak flow differences are very low in 1988 (Figure 47). January 1993 precipitation brought an instant high peak of more than 700 m<sup>3</sup>/sec (Figure 48). In the

1995 (Figure 49) five peaks were observed even though the total precipitation had been of the order of 200 mm to 400 mm.

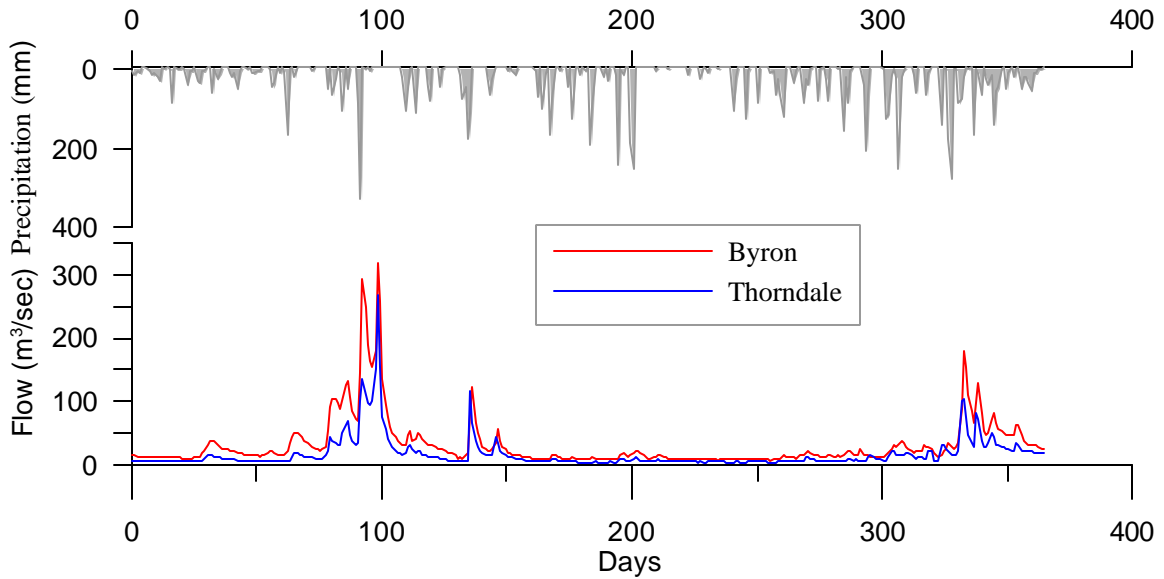


Figure 42: 1970 observed hydrographs at Byron and Thorndale and total precipitation at London, Ontario

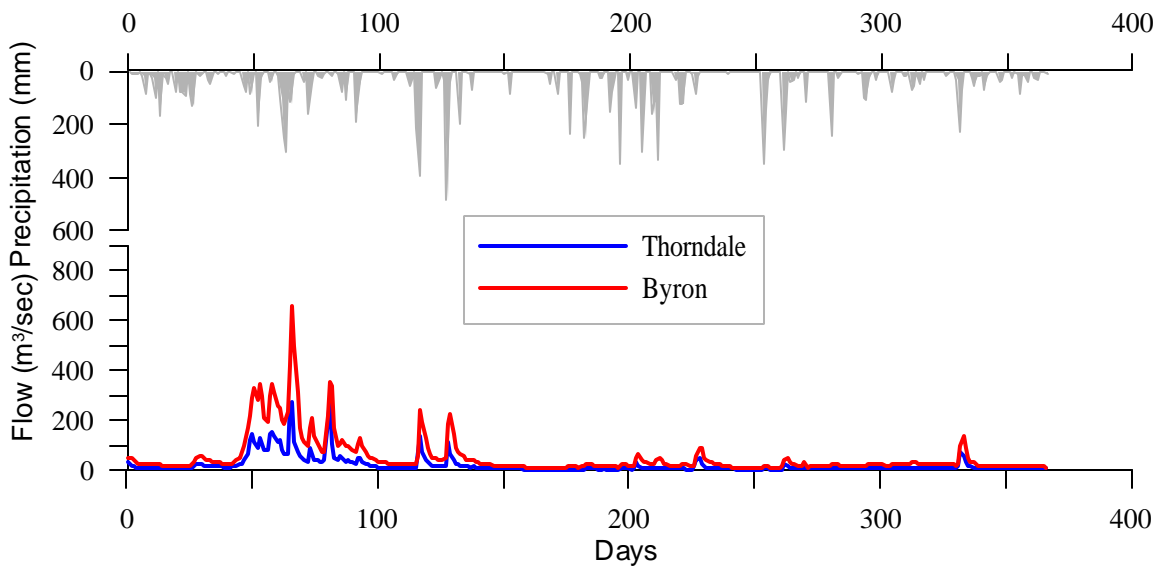


Figure 43: 1976 observed hydrographs at Byron and Thorndale and total precipitation at London, Ontario

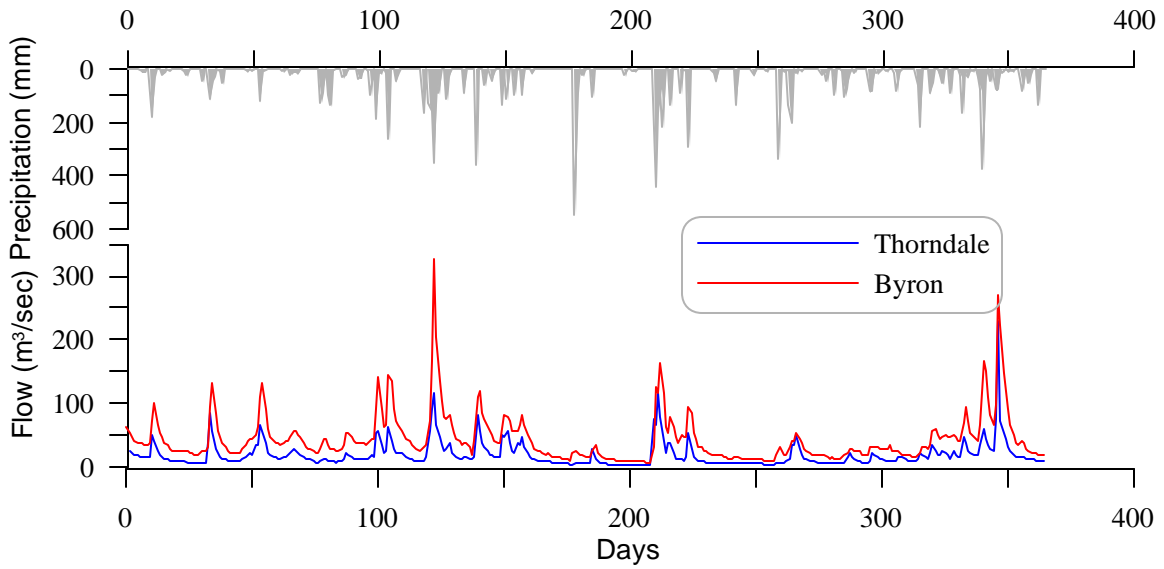


Figure 44: 1983 observed hydrographs at Byron and Thorndale and total precipitation at London, Ontario

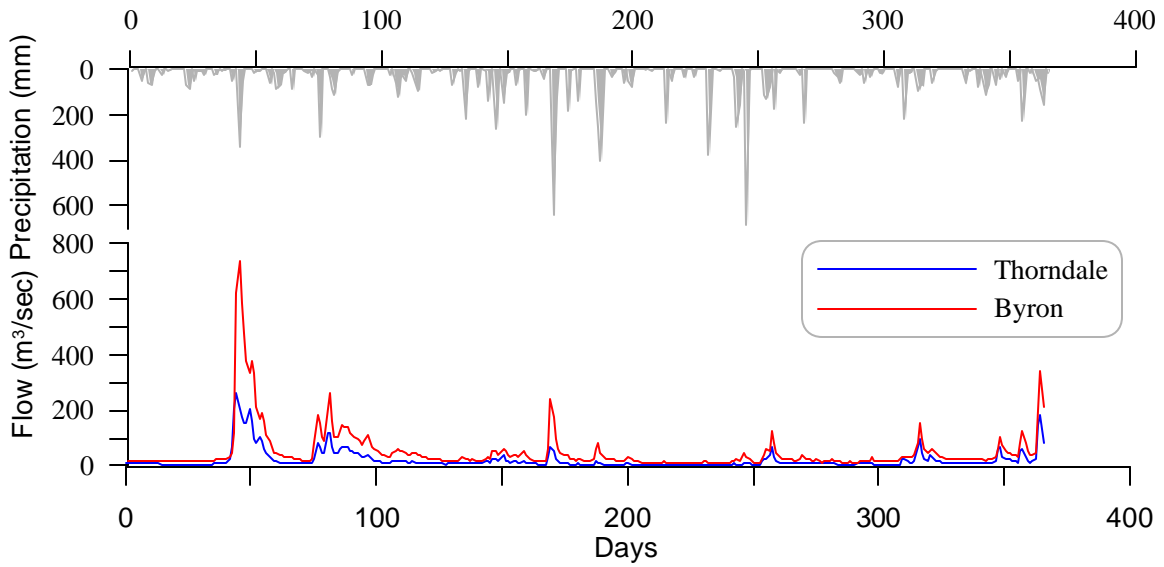


Figure 45: 1984 observed hydrographs at Byron and Thorndale and total precipitation at London, Ontario

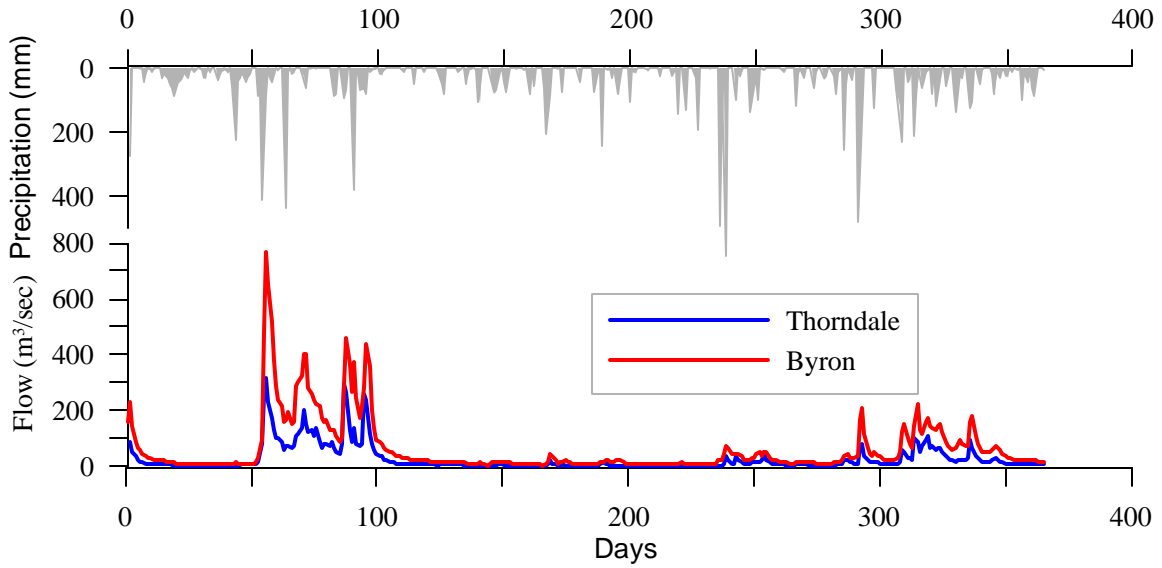


Figure 46: 1985 observed hydrographs at Byron and Thorndale and total precipitation at London, Ontario

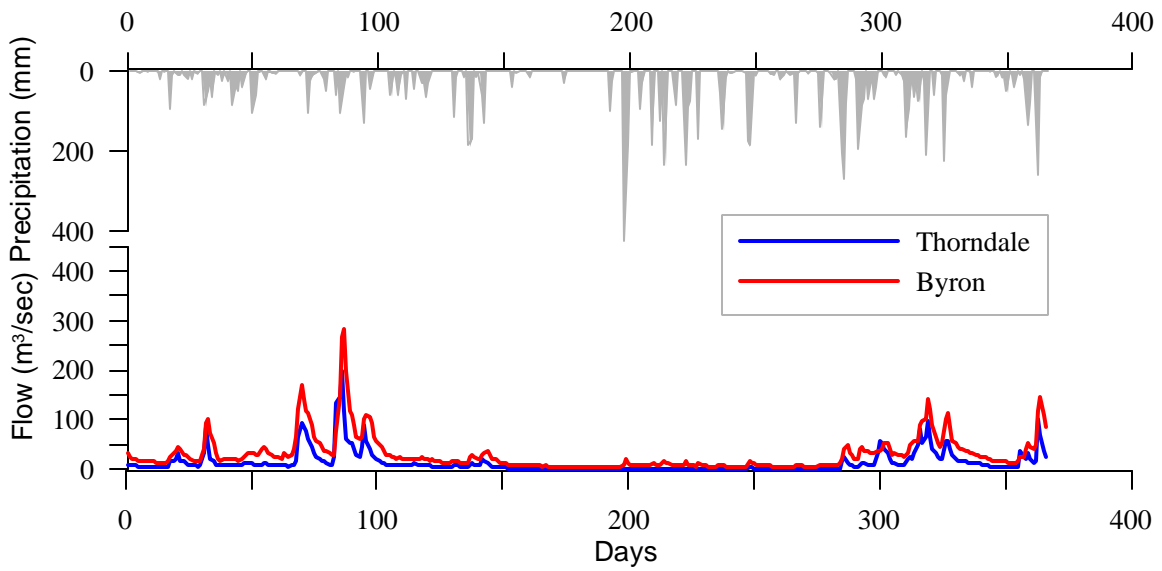


Figure 47: 1988 observed hydrographs at Byron and Thorndale and total precipitation at London, Ontario

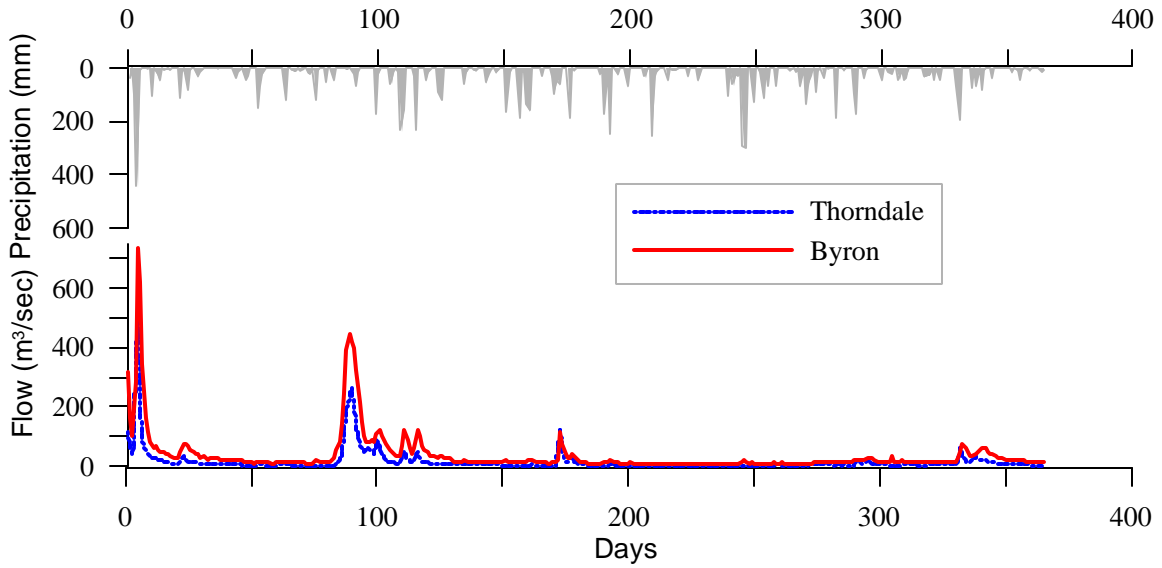


Figure 48: 1993 observed hydrographs at Byron and Thorndale and total precipitation at London, Ontario

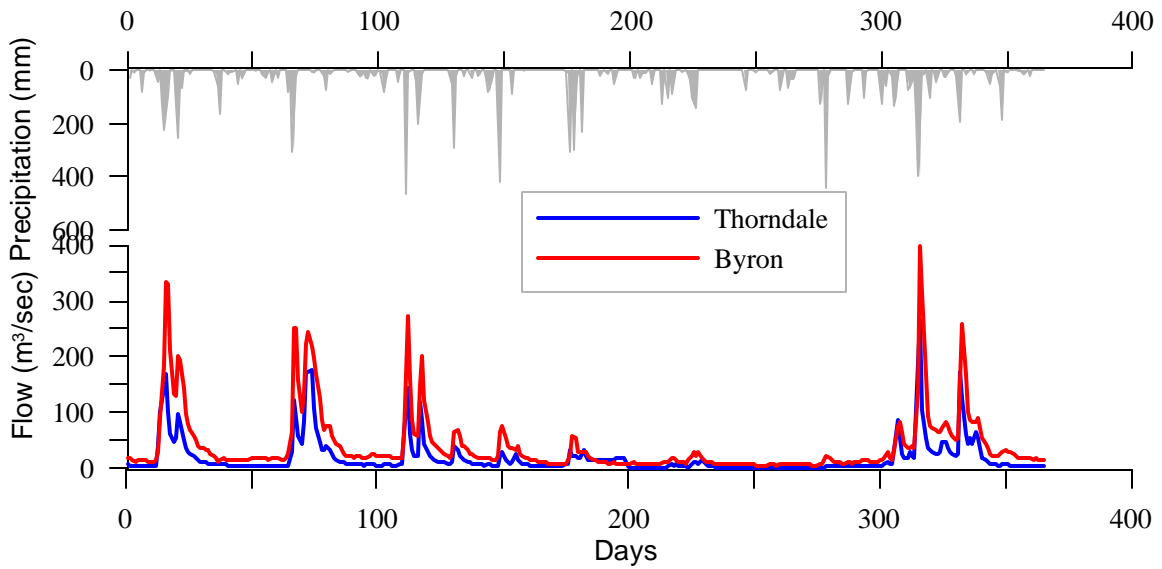


Figure 49: 1995 observed hydrographs at Byron and Thorndale and total precipitation at London, Ontario

In 1997 (Figure 50), too, despite the total precipitation being as low as below 200 mm during the beginning of the year there are instant high flows of more than 800 m<sup>3</sup>/sec at that time.

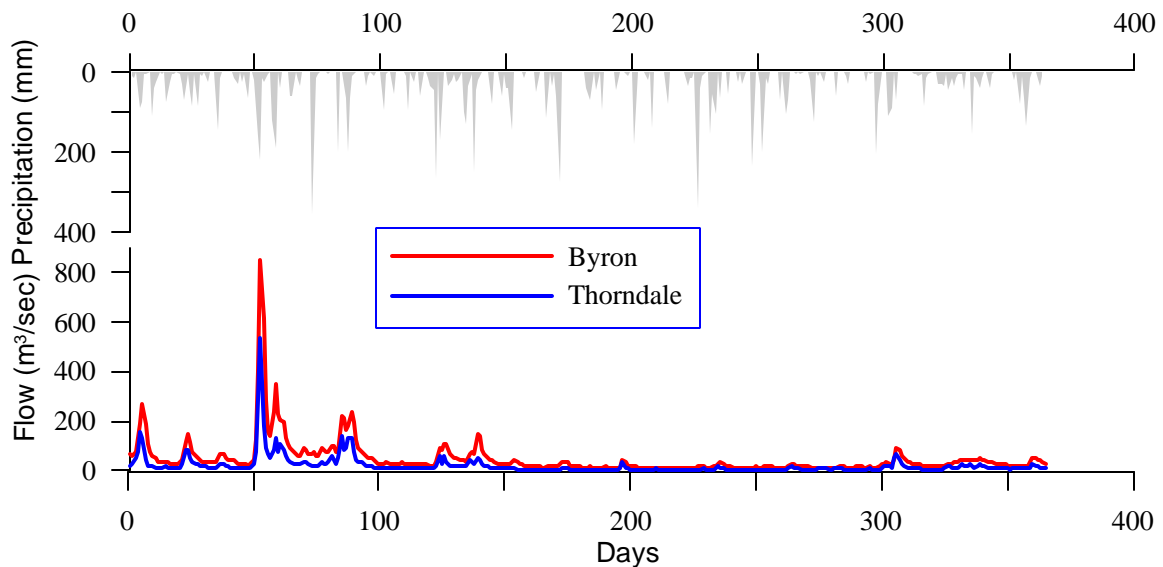


Figure 50: 1997 observed hydrographs at Byron and Thorndale and total precipitation at London, Ontario

### 6.2.3 Integration of remote sensing images and hydrologic data analysis

The remote sensing images, when classified for land use classes (woods, row crop and legume grasses, small grain or grass, fallow land, urban/city, homestead and water), give an indication that there has been major increase in urban sprawl over past three decades. Though there was a drop in wooded area in 1990 (11.98%) compared to 1974 (24.01%), it rose again in 2000 (13.06%) by nearly 1% of the watershed area. Looking at the hydrologic data, it can be seen that whereas, in 1970 (Figure 40) a total precipitation of

nearly 400 mm resulted in 350 m<sup>3</sup>/sec of peak flow, in 1997 (Figure 48) about 200 mm of total precipitation brought about more than 800 m<sup>3</sup>/sec of river flows at Byron (outlet point of UTR watershed). Similar trend can be seen in other years too, except for the fact that 1988 and 1989 were dry years according to UTRCA report (<http://www.thamesriver.on.ca>). So, it can be inferred that increase in impervious area enhances the river flows considerably.

#### *6.2.4 Discussion of Results*

Results presented in Table 2 and Figures 36-38 show that tremendous urban development has taken place in the watershed over three decades. Areas covered by woods came down in 1983 but rose again in the year 2000, probably due to the conservation measures taken by the provincial government and environmental groups after mid-70s (UTRCA, 1975). The significant difference in the percentage of row crops and legume grasses could be attributed to the difference in image acquisition months in 1983 and 2000. The variation in small grains or grass category shows slightly mixed signals that it could either be attributed to the difference in image acquisition time or some changes in the land use (from grass to urban and industrial development). Increase in the fallow land in 2000 as compared to 1974 could be justified by the fact that the crops were harvested in September and the 2000 image was taken in October. Homestead percentage drops gradually over the decades, indicating that farmers have moved to towns indulging in other professions and selling their lands to developers. Surface water area appears to be decreasing over the years – from 3.65% in 1974 to 2.73% in 2000.



Cropping is a dynamic process, which keeps changing several times during the year and the timing of the three remote sensing images do not match, therefore, not much can be concluded about the crops, small grains and fallow land classes. Lots of wooded regions have been cleared up for urban development in and around London city in UTR watershed and number of homestead have reduced considerably. Considering the awareness regarding conserving the forests that came into effect in late 70s (UTRCA, 1975), the rise in woods (dense forested area) is a positive sign, which conveys the message of successful implementation of UTR conservation authorities' policies. Similarly, new policies can be brought into affect to balance the urban and industrial development as a measure to keep the direct runoff under control and hence mitigate the chances of occurrences of floods during high intensity storms.

## **7. CONCLUDING REMARKS**

Natural disasters cause damage to life and property all over the world in various forms. The pressure on the earth's resources caused by increased population has resulted in increased vulnerability of human and their infrastructure to the natural hazards, which have always existed. The result is a dynamic equilibrium between these forces in which scientific and technological development plays a major role. Recurring occurrences of earthquakes, floods, landslides and forest fires need to be studied using today's advanced technology to find effective preventive measures. Space technology can help the disaster mitigation process through better future scenario predictions; detection of disaster prone areas; location of protection measures and safe alternate routes etc. Post-disaster satellite

data acquisition helps in disaster recovery; damage claim process and fast compensation settlement.

This report presents an account of existing space satellites orbiting the Earth to monitor its resources and changes that are taking place continually. Various satellites and sensors on-board provide with numerous possibilities of analyzing the data for disaster prediction and mitigation purposes. The nature of the natural disasters determines the suitability of sensor types, spectral bands, active or passive radar data and their spectral, temporal and spatial resolutions. Impact of land use on natural disasters and ability to predict them would be one of the main contribution of remote sensing technology in this century. Integration of remote sensing with GIS and web technology makes it an extremely powerful tool to identify indicators of potential disasters. Information sharing through Internet reduces data acquisition time and thus providing efficient way to carry out real-time disaster predictions (floods, forest fire, tsunami and hurricane etc.). Changing land use and assessment of its impact on the system in general within reasonable time frame and with greater degree of accuracy becomes possible with new technology.

Over the last three decades urban development has taken place everywhere in general. From conservation point of view the planning for developments is vital. In Upper Thames River watershed drastic land use changes have taken place over three decades. Whether or not these changes affect the river flows (leading to possibility of floods) has been discussed in this report. The Upper Thames River watershed case study clearly demonstrates that urban area has increased to 22.25% of the total watershed area in the

year 2000 compared to only 10.07% in 1974. According to natural hydrological phenomena, due to increased impervious area precipitation responds quickly reducing the time to peak and producing higher peak-flows in the drainage channels. Figures 42 – 50 illustrate this phenomenon through the hydrographs plotted using observed hydrologic and meteorological time series. Quantity of available surface water appears to be reducing slightly over the decades (3.65% in 1974 to 2.73% in 2000). Forests are being cut down continuously at an alarming rate reducing the forest reserves to a mere 13.06% at present. With the help of remote sensing and GIS technology the Upper Thames River watershed could be studied efficiently in lesser time compared to conventional methods. To update the database on land use in the watershed, all we would need to do is acquire more recent satellite imagery and carry out the land use classification. The case study is an example of how remote sensing and GIS technology can help in understanding the development pattern in a region and its affect on the hydrology of the area so as to help the authorities in forming the conservation policies with respect to land use.

The beneficiaries of new technology are almost everyone, namely, the people, government, and private insurance industry. It is crucial to know which of the areas are at high risk and which ones are at relatively lower risk. Investment towards making use of the space technology is worth because improvement in instrumentation and real time prediction will bring about reduction in disaster damages; better prediction; accurate and timely damage estimation; and improved decision making in planning stages.

Conventionally, flood emergency management, both public and private usually responds to crises rather than being concerned with the broader issues of vulnerability and its management (Shrubsole, 2001). Its time this culture changed a little so other alternatives for mitigation of flood damages, land slides and soil erosion, such as, planned land use, should be explored, proposed and implemented. The future is promising with the new generation of very high-resolution satellites, like, IKONOS, TSINGHUA and QUICKBIRD and many more coming future years. They will provide the daily high-resolution imaging of the world to track natural and human-made disasters.

## REFERENCES:

- Barber, D.G., Hochheim, K.P., Dixon, R., Mosscrop, D.R. and McMullan, M.J. (1996). "The Role of Earth Observation Technologies in Flood Mapping: A Manitoba Case Study". *Canadian Journal of Remote Sensing*, 22(1), 137-143.
- Barrett, E.C., Beaumont, M.J. and Herschy, R.W. (1990). "Satellite Remote Sensing for Operational Hydrology: Present Needs and Future Opportunities." *Remote Sensing Review*, 4(2), 351-466.
- Bernier, M. and Fortin, J.P. (1998). "The Potential of Times Series of C-Band SAR Data to Monitor Dry and Shallow Snow Cover." *IEEE Trans. Geo. Sc. & Rem. Sen.*, 36(1), 226-243.
- Birk, R.J. and Foresman, T. (2000). "Introduction to Special Issue Decision Support System" *J. Amer. Soc. PE&RS*, 66(10).
- Borneman, R. (1988). "Satellite Rainfall Estimating Program of NOAA/NESDIS Satellite Analysis Branch." *National Weather Digest*, 13(2), 7-15.
- Brakenridge, G.R., Tracy, B.T. and Knox, J.C. (1998). "Orbital SAR Remote Sensing of a River Flood Wave." *Int. J. Rem. Sen.*, 19(7), 1439-1445.
- Brakenridge, G.R., Tracy, B.T. and Knox, J.C. (1998). "Orbital SAR Remote Sensing of a River Flood Wave." *Int. J. Rem. Sen.*, 19(7), 1439-1445.
- Bruynzeel, L.A. (1990). Hydrology of moist tropical forests and effects of conversion: a state of knowledge review. UNESCO, 224.
- Colby, J.D., Wang, Y. and Mulcahy, K. (1999). "Hurricane Floyd Flood Mapping Integrating LANDSAT 7 TM Satellite Imagery and DEM Data." <http://www.colorado.edu/hazards/qr/qr126/qr126.html>.

Company Starts Building JERS-1 Data Processor.” *Space News*, 10-16 April.

*COSPAR Advanced Space Research* Vol. 15., No. 11: 3-14. Singh, R.P., and R.

Furrer, eds. Proceedings of the A3.2 Meeting of COSPAR Scientific Commission.

Great Britain: Pergamon 1994.

Davis, N.W. (1993). “Japan Stresses Multisatellite Remote Sensing.” *Aerospace America*, p28.

Dedieu, J.P., Bernier, M., Fortin, J.P., Sève, D.D. and Quevillon, P. (1997). “Remote Sensing of Snow Cover by Radarsat in the French Alps.” <http://www.rsi.ca/adro/adro/abstracts/076.html>.

Dutta, D. and Herath, S. (1999). “Global Flood Disasters During 1997-1998.” International Center for Disaster – Mitigation Engineering Institute of Industrial Science <http://incede.iis.u-tokyo.ac.jp>.

Eastman, J.R. (2001) Guide to GIS and Image Processing Volume 2, Idrisi Manual version 32.20, 65.

ERDAS Field Guide, 1991, Second Edition, Version 7.5.

Feidas, H.N., Cartalis. C. and Cracknell, A.P. (2000). “Use of METEOSAT Imagery to Define Clouds Linked with Floods in Greece.” *Int. J. Rem. Sen.*, 21(5), 1047-1072.

Feidas, H.N., Cartalis. C. and Cracknell, A.P. (2000). “Use of METEOSAT Imagery to Define Clouds Linked with Floods in Greece.” *Int. J. Rem. Sen.*, 21(5), 1047-1072.

Fukami, K., Kodama, H., Matsuura, T., Kaneki, M., Koike, T., Tadono, T., Ujihashi, Y., Kondoh, A., Ohno, H., and Kamibayashi, N. (1999). “Relationship Between Snow Physical Properties and Microwave Backscatters Observed by Radarsat-SAR over the Hokuriku District in Japan.” <http://www.rsi.ca/adro/adro/abstracts/112.html>.

- Gorte, B.G.H. (2000). "Land-use and Catchment Characteristics" in Remote Sensing in Hydrology and Water Management, eds., Shultz, G.A. and Engman, E.T., Springer, 133-156.
- Hillard, U., Davis, L., Nijssen, B. and Lettenmaier, D.P. (1999). "Determination of Snow Cover Distribution and Snow Melt Rates in Central Canada Using Radarsat1." <http://www.rsi.ca/adro/adro/abstracts/286.html>.
- IRS-1D Handbook (1997). National Remote Sensing Agency, Dept. Space, Govt. India, India.
- Johnson, N. and Rodvold, D. (1994). Europe and Asia in Space 1993-1994 (<http://fas.org/spp/guide/japan/earth/mos.htm>).
- Kundzewicz, Z.W., Rosbjerg, D., Simonovic, S.P. and Takeuchi, K. (eds.) (1993) "Extreme Hydrological Events: Precipitation, Floods and Droughts." IAHS Publication No.213, 21-32.
- Lanza, L. and Conti, M. (1994). "Remote Sensing and GIS: Potential Application for Flood Hazard Forecasting." *EGIS*. <http://www.odyssey.maine.edu/gisweb/spatdb/egis/eg94208.html>
- Lardy, M. and Sigaud, L. (1995) <http://SPOTimage.fr/home/appli/hazard/aoba/aoba.htm> (02 Nov 2000)
- Liew, S.C., Kwoh, L.K., Padmanabhan, K., Lim, O.K. and Lim, H. (1999). "Monitoring Vegetation Cover Changes in Peat Swamp Area of Central Kalimantan Using ERS Interferometric Synthetic Aperture Radar." *Int. Conf. And Workshop on Tropical Peat Swamps – Safeguarding a Global Natural Resource*, Penang, Malaysia.

Maxfield, A.W. (1999). "Wet Snow Radar Maps of the Rocky Mountains.",  
<<http://www.rsi.ca/adro/adro/abstracts/409.html>>.

Meijerink, A.M.J. and Maathuis, B. H.P. (1997). Use of Remote Sensing to assess flood damage to rice lands caused by accelerated erosion and neo-tectonics, Komering River, Sumatra. River Flood Disasters. Proc. ICSU SC/IDNDR. IHP/OHP-Berichte, Sonderheft 10, Koblenz, pp. 97-105.

Metternicht, G.I. and Zinck, J.A. (1998). "Evaluating the Information Content of JERS-1 SAR and LANDSAT TM Data for Discrimination of Soil Erosion Features." *J. Amer. Soc. PE&RS*, 53(3), 143-153.

Murphy, M., Martini, I.P. and Protz, R., (1998). "Characterization of Seasonal Backscatter Change in Subarctic Peatlands and River Ice Breaking using Radarsat Data." <http://www.rsi.ca/adro/adro/abstracts/475.html>.

Nagler, T., Rott, H. and Glendinning, G. (1998). "Snowmelt Modelling Using Radarsat Data." <<http://www.rsi.ca/adro/adro/abstracts/414.html>>.

NASDA, (1992). National Space Development Agency of Japan. p21-22

NASDA, 1990

Nico, G., Pappalepore, M., Pasquariello, G., Refice, A. and Samarelli, S. (2000). "Comparison of SAR amplitude vs. Coherence Flood Detection Method – A GIS Application." *Int. J. Rem.Sen.*, 21(8), 1619-1631.

OAS (1990). Disaster, Planning and Development: Managing Natural Hazards to Reduce Loss. Dept. Regional Development and Environment. Organizaion of American States. Washington, USA, 80.



- Okamoto, K., Yamakawa, S. and Kawashima, H. (1998). "Estimation of Flood Damage to Rice Production in North Korea in 1995." *Int. J. Rem. Sen.*, 19(2), 365-371.
- Oppenheimer, C. (1997). "Remote Sensing of the Colour and Temperature of Volcanic Lakes." *Int. J. Rem. Sen.*, 18(1), 5-37.
- Pankiewicz, G.S. (1997). "Neural Network Classification of Convective Airmasses for a Flood Forecasting System." *Int. J. Rem. Sen.*, 18(4), 887-898.
- Pankiewicz, G.S. (1997). "Neural Network Classification of Convective Airmasses for a Flood Forecasting System." *Int. J. Rem. Sen.*, 18(4), 887-898.
- Petkov, L., Pieri, M., Maselli, F. and Maracchi, G. (1996). "Study and Modelling of Temperature Spatial Variability by NOAA-AVHRR Thermal Imagery." *J. Amer. Soc. PE&RS*, 51(3), 127-136.
- Rau, F. and Saurer, H. (1998). "Investigations into Snow Cover Dynamics on Two Glaciers in the Central Marguerite Bay (Antarctic Peninsula) using Radarsat SAR Imagery." <http://www.rsi.ca/adro/adro/abstracts/540.html>.
- Richards, P.B., (1982). "The Utility of LANDSAT-D and Other Satellite Imaging Systems in Disaster Management." Final Report, NASA Goddard Space Flight Center Disaster Management Workshop, NASA DPR S-70677, Washington, D.C., Naval Research Laboratory, 29-30.
- Riley, R.H., Phillips, D.L., Schuft, M.J. and Garcia, M.C. (1997). "Resolution and Error in Measuring Land-Cover Change: Effects on Estimating Net Carbon Release from Mexican Terrestrial Ecosystems." *Int. J. Rem. Sen.*, 18(1), 121-137.
- Saatchi, S.S., Nelson, B., Podest, E. and Holt, J. (2000). "Mapping Land Cover Types in the Amazon Basin Using 1km JERS-1 Mosaic." *Int. J. Rem. Sen.*, 21(6), 1201-1234.

- Saatchi, S.S., Nelson, B., Podest, E. and Holt, J. (2000). "Mapping Land Cover Types in the Amazon Basin Using 1km JERS-1 Mosaic." *Int. J. Rem. Sen.*, 21(6), 1201-1234.
- Sabins, F.F., (1986). "Remote Sensing: Principles and Interpretations." New York, W.H. Freeman.
- Saders, R. and Tabuchi, S. (2000). "Decision Support System for Flood Risk Analysis for the River Thames, United Kingdom." *J. Amer. Soc. PE&RS*, 66(10).
- Schjødt-Osmo and Engeset (1999). "Remote Sensing and Snow Monitoring: Application to Food Forecasting." (< <http://webben.nve.no/hydrologi/bre/remote/ewra97.html>>).
- Schjødt-Osmo and Engeset (1999). < <http://webben.nve.no/hydrologi/bre/remote/ewra97.html>>.
- Shrubsole, D. (2001) "The cultures of flood management in Canada: Insights from the 1997 Red River experience." *Canadian Water Resources Journal*, 26(4), 461-479.
- Simonovic, S.P. and Huang, P. (1999). "Prototype Virtual Database Development for Management of Floods in the Red River Basin." *CWRA- Manitoba Branch Conference Winnipeg MB, Red River Flooding: Managing Decreasing Our Risks*, pp. IX-1- IX-12.
- Simonovic, S.P., (1999). "Decision Support System for Flood Management in the Red River Basin." *Canadian Water Resources Journal*, Vol.24, No.3, 203-223.
- Spaceflight* (1987). "Japan's New Space Bid". p.138-141.
- Stussi, N., Kwoh, L.K., Liew, S.C., Singh, K. and Lim, H. (1996). "ERS-1/2 Interferometry: Some Results on Tropical Forest." *Fringe 96-ESA Workshop*, Remote Sensing Laboratories, U. Zurich, Switzerland.

- Sugumaran, R., Davis, C., Meyer, J., Prato, T. and Fulcher C. (2000). "Web-Based Decision Support Tool for Floodplain Management Using High-Resolution DEM." *J. Amer. Soc. PE&RS*, 66(10).
- Townsend, P.A. and Walsh, S.J. (1998). "Modeling Floodplain Inundation Using and Integrated GIS with Radar and Optical Remote Sensing." *Geomorphology*, 21(1998)295-312.
- UNDRO (1991). Mitigating Natural Disasters. Phenomena, Effects and Options. United Nations Disaster Relief Co-ordinator, United Nations, New York, 164.
- UTRCA publication, 1955, Brief on flood control measures for the Upper Thames Watershed.
- UTRCA publication, 1975, London valley lands study.
- UTRCA publication, 1994, Strategic plan, Upper Thames River Conservation Authority.
- UTRCA publication, Population projections for the Upper Thames Basin.
- Verstappen, H. Th., (1995) Aerospace Technology and Natural Disaster Reduction.

## **OTHER WEBSITES CITED**

- *<http://hsb.gsfc.nasa.gov>*
- *<http://seaspace.esa.int8000/>*
- *<http://www.ccrs.nrcan.gc.ca>*
- *<http://www.colorado.edu/hazards/>*
- *<http://www.fema.gov/library>*
- *<http://www.hohrc.nws.gov>*
- *<http://www.nnic.noaa.gov/socc>*
- *<http://www.spaceimaging.com>*
- *<http://www.usgs.gov>*
- *<http://www.oas.org/usde/>*
- *<http://www.digitalglobe.com>*